

Adaptive finite element approximations of the first eigenpair associated with p -Laplacian

Guanglian Li¹ Jing Li² Julie Merten³ Yifeng Xu⁴ Shengfeng Zhu⁵

Abstract

In this paper, we propose an adaptive finite element method for computing the first eigenpair of the p -Laplacian problem. We prove that starting from a fine initial mesh our proposed adaptive algorithm produces a sequence of discrete first eigenvalues that converges to the first eigenvalue of the continuous problem and the distance between discrete eigenfunctions and the normalized eigenfunction set corresponding to the first eigenvalue in $W^{1,p}$ -norm also tends to zero. Extensive numerical examples are provided to show the effectiveness and efficiency.

Keywords: p -Laplacian, first eigenvalue, a posteriori error estimator, adaptive finite element method, convergence

MSC (2020): 65N12, 65N25, 65N30, 65N50, 35P30

1 Introduction

In this paper, we consider the eigenvalue problem of the p -Laplacian operator with homogeneous Dirichlet boundary condition:

$$\begin{cases} -\nabla \cdot (|\nabla u|^{p-2} \nabla u) = \lambda |u|^{p-2} u & \text{in } \Omega, \\ u = 0 & \text{on } \partial\Omega, \end{cases} \quad (1.1)$$

where Ω is an open bounded Lipschitz polygonal/polyhedral connected domain in \mathbb{R}^d ($d = 2, 3$) and $1 < p < \infty$. From the perspective of applications, the p -Laplacian operator arises from non-Newtonian fluids [38] and power-law materials [6]. As usual, integration by parts yields the weak formulation of (1.1): Find $(\lambda, u) \in \mathbb{R} \times V$ such that

$$\int_{\Omega} |\nabla u|^{p-2} \nabla u \cdot \nabla v dx = \lambda \int_{\Omega} |u|^{p-2} u v dx \quad \forall v \in V. \quad (1.2)$$

Here we denote $V := W_0^{1,p}(\Omega)$.

The existing theory developed in [36, 46, 47] asserts that Problem (1.2) has a nondecreasing sequence of positive eigenvalues $\{\lambda_n\}_{n \geq 1}$ diverging to $+\infty$. It should be noted that the first eigenvalue λ_1 is simple and isolated [46, 47], and is equivalent to the minimum of the Rayleigh quotient

$$\lambda_1 = \inf_{v \in V \setminus \{0\}} \mathcal{J}(v) := \frac{\int_{\Omega} |\nabla v|^p dx}{\int_{\Omega} |v|^p dx}. \quad (1.3)$$

¹Department of Mathematics, The University of Hong Kong, Hong Kong Special Administrative Region, China. (lotusli@maths.hku.hk)

²School of Mathematical Sciences, East China Normal University, Shanghai 200241, China. (betterljing@163.com)

³Computational and Numerical Mathematics, Bernoulli Institute, University of Groningen, the Netherlands. (j.y.merten@rug.nl)

⁴Corresponding author. Department of Mathematics & Scientific Computing Key Laboratory of Shanghai Universities, Shanghai Normal University, Shanghai 200234, China. (yfxu@shnu.edu.cn)

⁵Key Laboratory of MEA (Ministry of Education) & Shanghai Key Laboratory of PMMP, School of Mathematical Sciences, East China Normal University, Shanghai 200241, China. (sfzhu@math.ecnu.edu.cn)

The existence of a minimizer to Problem (1.3) can be established by the standard minimization approach (cf. [8, 47]). Moreover, the reciprocal of λ_1 is the best constant in Poincaré inequality, which implies that $\lambda_1 > 0$. A normalized eigenfunction set with respect to λ_1 is defined as

$$E_{\lambda_1} := \left\{ u \in V \mid \int_{\Omega} |\nabla u|^{p-2} \nabla u \cdot \nabla v dx = \lambda_1 \int_{\Omega} |u|^{p-2} u v dx, \forall v \in V, \|u\|_{L^p(\Omega)} = 1 \right\}.$$

Some attempts have been made in numerically computing eigenpairs of Problem (1.1) [10, 11, 13, 39, 44, 60]. But due to the degenerate structure of the operator and the existence of possible reentrant corners in the computational domain Ω , the solution to Problem (1.1) features local singularities. As a remedy, adaptive techniques are preferred in numerical simulation for accuracy and efficiency. Generally speaking, a standard adaptive finite element method (AFEM) comprises the following four modules in every loop:

$$\text{SOLVE} \rightarrow \text{ESTIMATE} \rightarrow \text{MARK} \rightarrow \text{REFINE}. \quad (1.4)$$

The most prominent advantage of AFEM is to make efficient use of computer resources to attain the given error tolerance with minimum degrees of freedom, so it has become an effective tool in practice of scientific computing and engineering. Since the seminal work [7] by Babuška and Rheinboldt in 1978, there has been much and rapid progress in the mathematical theory of this field. In particular, the understanding of a posteriori estimation, the main ingredient in the module ESTIMATE, is now on a mature level; see e.g. [2, 58]. Moreover, great efforts have been put into the study of AFEM itself in terms of convergence and complexity over the past three decades. For linear elliptic problems one may refer to two survey papers [16, 52] and the references therein for an overview. In the case of linear or nonlinear eigenvalue problems, where nonlinearity consists in low order terms, we are aware that existing works are only limited to the linear Laplacian/diffusion/bi-Laplacian operator; see [12, 14, 17–19, 22–25, 28, 29, 31–35]. For the nonlinear Laplacian equation, we mention [9, 21, 30, 48, 49, 57] for results on a posteriori error estimation and adaptive computations.

The aim of this paper is to develop adaptive finite element approximations of the first eigenvalue λ_1 to Problem (1.1). To be specific, we propose Algorithm 1 of standard form (1.4), which facilitates implementation in practical applications, for the first eigenpair of Problem (1.2) in Section 3 and establish the convergence of its resulting first discrete eigenpairs $\{(\mu_k, u_k)\}_{k \geq 0}$ in Section 4. It is demonstrated in Theorem 4.3 that the whole sequence $\{\mu_k\}_{k \geq 0}$ converges to λ_1 and the $W^{1,p}(\Omega)$ -norm between $L^p(\Omega)$ -normalized sequence $\{u_k\}_{k \geq 0}$ and E_{λ_1} tends to zero.

In addition to standard arguments for linear problems [34, 35], minimization techniques for nonlinear elliptic problems [3, 8] are utilized to deal with the nonlinear structure of Problem (1.1) in the convergence analysis. By introducing an auxiliary minimization problem (4.1) over the limiting space given by the adaptive process (1.4), we first prove in Theorem 4.1 and Theorem 4.2 that the sequence of discrete eigenpairs $\{(\mu_k, u_k)\}_{k \geq 0}$ converges (up to a subsequence) to $(\mu_{\infty}, u_{\infty})$, where μ_{∞} denotes the minimum to Problem (4.1), and u_{∞} the $L^p(\Omega)$ -normalized minimizer. Then we further prove $(\mu_{\infty}, u_{\infty})$ satisfies the variational formulation (1.2) (see Section 4.2 and Step 1 in the proof of Theorem 4.3), which indicates that u_{∞} is a critical point of \mathcal{J} over V . Finally, the convergence of the whole sequence $\{(\mu_k, u_k)\}_{k \geq 0}$ to λ_1 and E_{λ_1} is proved under the assumption that the initial mesh is sufficiently fine (see Step 2 and Step 3 in the proof of Theorem 4.3). The unquantifiable fineness requirement on the initial mesh is precisely undesirable in adaptive computations, but it seems inevitable even in the analysis of AFEM for linear eigenvalue problems. It should also be pointed out that some computable quantities adopted in the module ESTIMATE are derived (see the proof of Lemma 4.2), although they do not provide an upper bound of the error, in our convergence analysis, where a practical assumption (see (3.2) in Algorithm 1) imposed in the module MARK as for linear cases [34, 35] is utilized.

The remaining of this paper is organized as follows. A numerical scheme built on the finite element method for Problem (1.3) is presented in Section 2. In Section 3, we introduce a standard adaptive finite element method with a general yet reasonable requirement on the marking strategy, the convergence of which is investigated in Section 4. Section 5 deals with the implementation of our proposed algorithm and contains some numerical results illustrating the efficiency. The paper is ended with some concluding remarks in Section 6. Throughout the paper, we use standard notation for $L^p(\Omega)$ or $L^\infty(\Omega)$ space, the Sobolev space $W_0^{1,p}(\Omega)$ ($W^{2,\infty}(\Omega)$) and its dual space $W^{-1,q}(\Omega)$ with $q = p/(p-1) \in (1, \infty)$ as well as their related (semi-)norms. Moreover, the upper-case letter C , with or without subscript, denotes a generic constant independent of the mesh size and it may take a different value at each occurrence.

2 Discrete Problem

In this section, we introduce a discrete problem to approximate the minimization problem (1.3). For this purpose, let \mathcal{T} be a conforming triangulation of $\bar{\Omega}$ into a set of closed triangles or tetrahedra with a discretization parameter $h_T := |T|^{1/d}$ for each $T \in \mathcal{T}$. Let $V_{\mathcal{T}}$ be the associated conforming space of continuous piecewise linear functions vanishing on boundary $\partial\Omega$ given by

$$V_{\mathcal{T}} := \{v \in C(\bar{\Omega}) \mid v|_{\partial\Omega} = 0, v|_T \in P_1(T), \forall T \in \mathcal{T}\}.$$

Then the finite element approximation of (1.3) is seeking $u_{\mathcal{T}} \in V_{\mathcal{T}} \setminus \{0\}$, satisfying

$$\mu_{\mathcal{T}} := \mathcal{J}(u_{\mathcal{T}}) = \inf_{v \in V_{\mathcal{T}} \setminus \{0\}} \mathcal{J}(v). \quad (2.1)$$

Note that the property $V_{\mathcal{T}} \subset V$ implies that

$$0 < \lambda_1 \leq \mu_{\mathcal{T}}. \quad (2.2)$$

Theorem 2.1. *Let $\mu_{\mathcal{T}}$ be the solution to Problem (2.1), then $\mu_{\mathcal{T}}$ is positive and attained by some nonnegative function $u_{\mathcal{T}} \in V_{\mathcal{T}} \setminus \{0\}$.*

Proof. Our proof follows from the argument in [8], which is concerned with the continuous problem (1.3). The Poincaré inequality reads

$$\frac{\int_{\Omega} |\nabla u_{\mathcal{T}}|^p dx}{\int_{\Omega} |u_{\mathcal{T}}|^p dx} \geq C > 0 \quad \forall v \in V_{\mathcal{T}} \setminus \{0\},$$

which provides a positive lower bound. Hence, $\mu_{\mathcal{T}}$ is positive.

Let $\{v_m\}_{m \geq 0} \subset V_{\mathcal{T}} \setminus \{0\}$ be a minimizing sequence to Problem (2.1). Since $\{|v_m|\}_{m \geq 0}$ is also a minimizing sequence, then we can assume that $v_m \geq 0$ a.e. in Ω for all m . Moreover, the homogeneity of the objective functional \mathcal{J} allows for the normalization $\int_{\Omega} |v_m|^p dx = 1$. Consequently, the minimizing sequence $\{v_m\}_{m \geq 0}$ is bounded in the finite dimensional space $V_{\mathcal{T}}$. This guarantees the existence of a subsequence, still denoted by $\{v_m\}_{m \geq 0}$, and some $u_{\mathcal{T}} \in V_{\mathcal{T}}$, satisfying

$$v_m \rightarrow u_{\mathcal{T}} \text{ strongly in } W_0^{1,p}(\Omega), \quad v_m \rightarrow u_{\mathcal{T}} \text{ a.e. in } \Omega.$$

By this, we derive that $u_{\mathcal{T}} \geq 0$ a.e. in Ω , $\int_{\Omega} |u_{\mathcal{T}}|^p dx = 1$ and $\mathcal{J}(u_{\mathcal{T}}) = \lim_{m \rightarrow \infty} \mathcal{J}(v_m) = \mu_{\mathcal{T}}$. The proof is complete. \square

Theorem 2.1 implies that the discrete minimizer $u_{\mathcal{T}}$ can be normalized as $\|u_{\mathcal{T}}\|_{L^p(\Omega)} = 1$ in our adaptive algorithm below and the subsequent analysis. By the differential calculus for \mathcal{J} [8], it is easy to see that solution $(\mu_{\mathcal{T}}, u_{\mathcal{T}})$ to Problem (2.1) satisfies the discrete formulation of Problem (1.2),

$$\int_{\Omega} |\nabla u_{\mathcal{T}}|^{p-2} \nabla u_{\mathcal{T}} \cdot \nabla v dx = \mu_{\mathcal{T}} \int_{\Omega} |u_{\mathcal{T}}|^{p-2} u_{\mathcal{T}} v dx \quad \forall v \in V_{\mathcal{T}}. \quad (2.3)$$

3 Adaptive Finite Element Method

Let \mathbb{T} be the set of all possible conforming triangulations of $\overline{\Omega}$ obtained from some initial mesh \mathcal{T}_0 by successive use of bisection [43, 52, 55]. This refinement process ensures that the set \mathbb{T} is uniformly shape regular, i.e. the shape regularity of any $\mathcal{T} \in \mathbb{T}$ is uniformly bounded by a constant depending on the initial mesh \mathcal{T}_0 [52, 56]. $\mathcal{T}' \in \mathbb{T}$ is referred to as a refinement of $\mathcal{T} \in \mathbb{T}$ if \mathcal{T}' is produced from \mathcal{T} by a finite number of bisections. The collection of all interior faces in $\mathcal{T} \in \mathbb{T}$ is denoted by $\mathcal{F}_{\mathcal{T}}(\Omega)$ and the scalar $h_F := |F|^{1/(d-1)}$ stands for the diameter-equivalent mesh-size of each $F \in \mathcal{F}_{\mathcal{T}}(\Omega)$, which is associated with a fixed normal unit vector \mathbf{n}_F . The union of elements neighbouring some $T \in \mathcal{T}$ is denoted by D_T , i.e.

$$D_T = \bigcup_{T' \in \mathcal{T}: \partial T \cap \partial T' \neq \emptyset} T'.$$

First, let $(\mu_{\mathcal{T}}, u_{\mathcal{T}}) \in \mathbb{R} \times V_{\mathcal{T}}$ be the solution to Problem (2.1) with $\|u_{\mathcal{T}}\|_{L^p(\Omega)} = 1$ for $\mathcal{T} \in \mathbb{T}$. We define an element residual and a jump residual with respect to an element $T \in \mathcal{T}$ and a face $F \in \mathcal{F}_{\mathcal{T}}(\Omega)$ by

$$R_T(\mu_{\mathcal{T}}, u_{\mathcal{T}}) := \mu_{\mathcal{T}} |u_{\mathcal{T}}|^{p-2} u_{\mathcal{T}}, \quad J_F(u_{\mathcal{T}}) := [|\nabla u_{\mathcal{T}}|^{p-2} \nabla u_{\mathcal{T}}] \cdot \mathbf{n}_F$$

with

$$[|\nabla u_{\mathcal{T}}|^{p-2} \nabla u_{\mathcal{T}}] := (|\nabla u_{\mathcal{T}}|^{p-2} \nabla u_{\mathcal{T}})|_{F \subset \partial T^+} - (|\nabla u_{\mathcal{T}}|^{p-2} \nabla u_{\mathcal{T}})|_{F \subset \partial T^-}$$

denoting the jump across an interior face F shared by $T^+, T^- \in \mathcal{T}$. Then the local error indicator on each element $T \in \mathcal{T}$ is defined by

$$\eta_{\mathcal{T}}^q(\mu_{\mathcal{T}}, u_{\mathcal{T}}; T) := h_T^q \|R_T(\mu_{\mathcal{T}}, u_{\mathcal{T}})\|_{L^q(T)}^q + \sum_{F \subset \partial T \cap \Omega} h_F \|J_F(u_{\mathcal{T}})\|_{L^q(F)}^q \quad \text{with } q = p/(p-1). \quad (3.1)$$

Over some element patch $\mathcal{M} \subseteq \mathcal{T}$, the error estimator is defined by

$$\eta_{\mathcal{T}}(\mu_{\mathcal{T}}, u_{\mathcal{T}}; \mathcal{M}) := \left(\sum_{T \in \mathcal{M}} \eta_{\mathcal{T}}^q(\mu_{\mathcal{T}}, u_{\mathcal{T}}; T) \right)^{1/q}.$$

When $\mathcal{M} = \mathcal{T}$, we abbreviate $\eta_{\mathcal{T}}(\mu_{\mathcal{T}}, u_{\mathcal{T}}; \mathcal{T})$ to $\eta_{\mathcal{T}}(\mu_{\mathcal{T}}, u_{\mathcal{T}})$.

Next, we propose an AFEM for Problem (1.3). In what follows, all dependence on a triangulation \mathcal{T}_k is replaced by the mesh refinement level k in the subscript, e.g. $V_k := V_{\mathcal{T}_k}$.

Algorithm 1: AFEM for the 1st eigenvalue of p -Laplacian

- 1: (INITIALIZE) Specify an initial conforming mesh \mathcal{T}_0 and set counter $k := 0$.
- 2: (SOLVE) Solve Problem (2.1) on \mathcal{T}_k for $(\mu_k, u_k) \in \mathbb{R} \times V_k$ s.t., $\|u_k\|_{L^p(\Omega)} = 1$.
- 3: (ESTIMATE) Compute the error estimator $\eta_k(\mu_k, u_k; T)$ by (3.1) for each $T \in \mathcal{T}_k$.
- 4: (MARK) Mark a subset $\mathcal{M}_k \subseteq \mathcal{T}_k$ such that \mathcal{M}_k contains at least one element T_k with the largest error indicator over \mathcal{T}_k , i.e.

$$\eta_k(\mu_k, u_k; T_k) := \max_{T \in \mathcal{T}_k} \eta_k(\mu_k, u_k; T). \quad (3.2)$$

- 5: (REFINE) Refine each $T \in \mathcal{M}_k$ by bisection to get \mathcal{T}_{k+1} .
 - 6: Set $k := k + 1$ and go to Step 1.
-

We note that a general yet reasonable assumption is included in the module MARK of Algorithm 1. This requirement in marking elements for a further refinement helps to improve the computing efficiency in practical applications and is fulfilled by several popular marking strategies [52], e.g. the maximum strategy, the equi-distribution strategy, the modified equi-distribution strategy and the practical Dörfler's strategy. In the numerical implementation of Algorithm 1, a tolerance for the estimator or a bound for the number of DOFs is usually prescribed as a stopping criterion. Without it, an infinite sequence $\{\mu_k\}_{k \geq 0}$ is generated by Algorithm 1 and a natural question is whether it converges to the first eigenvalue of (1.1), which will be examined at extensive length in the next section. For this purpose, we end this section with a stability estimate for the local error indicator.

Lemma 3.1. *Let $\{(\mu_k, u_k)\}_{k \geq 0}$ be the sequence of discrete solutions generated by Algorithm 1. For any $T \in \mathcal{T}_k$, there holds*

$$\begin{aligned} \eta_k^q(u_k, \mu_k; T) &\leq C \left(h_T^q \|u_k\|_{L^p(T)}^p + \|\nabla u_k\|_{L^p(D_T)}^p \right), \\ \eta_k(u_k, \mu_k) &\leq \tilde{C}, \end{aligned} \quad (3.3)$$

where the constants C and \tilde{C} depend on μ_0 .

Proof. On the one hand, since $\|u_k\|_{L^p(\Omega)} = 1$ and since the sequence $\{V_k\}_{k \geq 0}$ is nested, then the discrete eigenvalues $\{\mu_k\}_{k \geq 0}$ form a monotonously decreasing positive sequence satisfying

$$|u_k|_{W^{1,p}(\Omega)}^p = \mu_k \leq \mu_0 \quad \forall k \geq 0. \quad (3.4)$$

Note that $q = p/(p-1) > 1$, then a straightforward calculation leads to

$$h_T^q \mu_k^q \int_T |u_k|^p dx \leq h_T^q \mu_0^q \|u_k\|_{L^p(T)}^p. \quad (3.5)$$

On the other hand, on each $F \in \mathcal{F}_k(\Omega)$ shared by two adjacent elements $T, T' \in \mathcal{T}_k$, an application of the scaled trace theorem [58] and the inverse estimate [27] reveals

$$\begin{aligned} h_F \| [|\nabla u_k|^{p-2} \nabla u_k] \cdot \mathbf{n}_F \|_{L^q(F)}^q &\leq 2^{q-1} h_F \left(\int_F |(|\nabla u_k|^{p-2} \nabla u_k)_T|^{\frac{p}{p-1}} ds + \int_F |(|\nabla u_k|^{p-2} \nabla u_k)_{T'}|^{\frac{p}{p-1}} ds \right) \\ &= 2^{q-1} h_F \left(\|(\nabla u_k)_T\|_{L^p(F)}^p + \|(\nabla u_k)_{T'}\|_{L^p(F)}^p \right) \\ &\leq C \|\nabla u_k\|_{L^p(T \cup T')}^p. \end{aligned}$$

Then we get

$$\sum_{F \subset \partial T \cap \Omega} h_F \int_F | [|\nabla u_k|^{p-2} \nabla u_k] \cdot \mathbf{n}_F |^{\frac{p}{p-1}} ds \leq C \int_{D_T} |\nabla u_k|^p dx.$$

This, together with (3.5), leads to the first assertion.

Summing up the first inequality in (3.3) over $T \in \mathcal{T}_k$, in combination with $h_T \leq \max_{T \in \mathcal{T}_0} h_T$, (3.4) and $\|u_k\|_{L^p(\Omega)} = 1$, yields the second assertion. This completes the proof. \square

4 Convergence

In this section, we are concerned with the convergence of Algorithm 1 in the sense that the sequence of discrete eigenvalues $\{\mu_k\}_{k \geq 0}$ converges to the first eigenvalue λ_1 of Problem (1.2) and

the distance in $W^{1,p}(\Omega)$ -norm between E_{λ_1} and the sequence of discrete eigenfunctions $\{u_k\}_{k \geq 0}$ tends to zero. As in [34, 35] for eigenvalue problems associated with the linear diffusion operator, our analysis starts with an artificial minimization problem in Section 4.1, with its solution being proved to be the limit of the sequence of discrete eigenfunctions generated by Algorithm 1. Then we invoke some auxiliary results on the error estimator $\eta_k(\mu_k, u_k)$ in Section 4.2, and finally prove the desired convergence in Section 4.3. It is interesting to note that $\eta_k(u_k, \mu_k)$ given by (3.1) is not a reliable estimator and the marking assumption (3.2) will play an important role in the subsequent analysis.

4.1 Limiting Behaviour

With the sequence of $\{V_k\}_{k \geq 0}$ generated by Algorithm 1, we define a limiting space $V_\infty := \overline{\bigcup_{k \geq 0} V_k}$ in $W^{1,p}(\Omega)$ -norm. It is not difficult to know that V_∞ is a closed subspace of V . We now consider a limiting minimization problem: find $u_\infty \in V_\infty$ such that

$$\mathcal{J}(u_\infty) = \inf_{v \in V_\infty \setminus \{0\}} \mathcal{J}(v). \quad (4.1)$$

Theorem 4.1. *Problem (4.1) has a nonnegative solution u_∞ in $V_\infty \setminus \{0\}$.*

Proof. Let $\{(\mu_k, u_k)\}_{k \geq 0}$ be the sequence of discrete solutions given by Algorithm 1. Since $\{V_k\}_{k \geq 0}$ is nested, then by (2.2) $\{\mu_k\}_{k \geq 0}$ is a decreasing sequence bounded from below by λ_1 . Consequently, there is $\mu_\infty > 0$ such that $\mu_k \rightarrow \mu_\infty$. The identity $\|u_k\|_{L^p(\Omega)} = 1$, together with $|u_k|_{W^{1,p}(\Omega)}^p = \mu_k$ in (3.4), leads to the assertion that $\{\|u_k\|_{W^{1,p}(\Omega)}\}_{k \geq 0}$ is bounded.

On one hand, note that V_∞ is a closed subspace of $W_0^{1,p}(\Omega)$, then the reflexivity and Sobolev compact embedding theorem [1] imply the existence of a subsequence $\{u_{k_j}\}_{j \geq 0}$ and some $u_\infty \in V_\infty$, satisfying

$$\begin{aligned} u_{k_j} &\rightarrow u_\infty \text{ weakly in } W_0^{1,p}(\Omega), \\ u_{k_j} &\rightarrow u_\infty \text{ strongly in } L^p(\Omega), \\ u_{k_j} &\rightarrow u_\infty \text{ a.e. in } \Omega. \end{aligned} \quad (4.2)$$

By $\|u_{k_j}\|_{L^p(\Omega)} = 1$ and the second (i.e. the strong) convergence in (4.2), we have

$$\|u_\infty\|_{L^p(\Omega)} = 1. \quad (4.3)$$

On the other hand, thanks to the definition of V_∞ , any $v \in V_\infty \setminus \{0\}$ admits a sequence $\{v_k\}_{k \geq 0} \subset \bigcup_{k \geq 0} V_k$ with each $v_k \in V_k$ such that

$$v_k \rightarrow v \text{ strongly in } W_0^{1,p}(\Omega). \quad (4.4)$$

As each u_k is a minimizer of \mathcal{J} over $V_k \setminus \{0\}$, then

$$\mathcal{J}(u_k) \leq \mathcal{J}(v_k). \quad (4.5)$$

Now using the first (i.e. the weak) convergence in (4.2) and collecting (4.3)-(4.5), we arrive at

$$\begin{aligned} \mathcal{J}(u_\infty) &= |u_\infty|_{W^{1,p}(\Omega)}^p \leq \liminf_{j \rightarrow \infty} |u_{k_j}|_{W^{1,p}(\Omega)}^p \\ &= \liminf_{j \rightarrow \infty} \mathcal{J}(u_{k_j}) \\ &\leq \limsup_{j \rightarrow \infty} \mathcal{J}(u_{k_j}) \\ &\leq \limsup_{k \rightarrow \infty} \mathcal{J}(u_k) \leq \limsup_{k \rightarrow \infty} \mathcal{J}(v_k) = \mathcal{J}(v) \quad \forall v \in V_\infty \setminus \{0\}. \end{aligned} \quad (4.6)$$

This implies that u_∞ is a minimizer over $V_\infty \setminus \{0\}$. As each u_k is nonnegative, the third pointwise convergence in (4.2) implies that $u_\infty \geq 0$ a.e. in Ω . This completes the proof. \square

Theorem 4.2. *Let $\{(\mu_k, u_k)\}_{k \geq 0}$ be the sequence of discrete solutions generated by Algorithm 1, then there holds*

$$\mu_k \rightarrow \mu_\infty = \mathcal{J}(u_\infty). \quad (4.7)$$

Moreover, there exists a subsequence $\{u_{k_j}\}_{j \geq 0}$ such that

$$\|u_{k_j} - u_\infty\|_{W^{1,p}(\Omega)} \rightarrow 0. \quad (4.8)$$

Proof. At the beginning of the proof of Theorem 4.1, we showed that there is $\mu_\infty > 0$ such that $\mu_k \rightarrow \mu_\infty$. Taking $v = u_\infty$ in (4.6) implies

$$\mu_{k_j} = \mathcal{J}(u_{k_j}) \rightarrow \mathcal{J}(u_\infty). \quad (4.9)$$

By the uniqueness of the limit, we conclude that $\mu_\infty = \mathcal{J}(u_\infty)$. For the second assertion, thanks to the uniform convexity of $W_0^{1,p}(\Omega)$ [1] and the weak convergence in (4.2), it suffices to prove the norm convergence $\|u_{k_j}\|_{W^{1,p}(\Omega)} \rightarrow \|u_\infty\|_{W^{1,p}(\Omega)}$, which is an immediate consequence of the $L^p(\Omega)$ strong convergence in (4.2), easy facts that $\mu_{k_j} = |u_{k_j}|_{W^{1,p}(\Omega)}^p$ and $\mathcal{J}(u_\infty) = |u_\infty|_{W^{1,p}(\Omega)}^p$ as well as (4.9). \square

Remark 4.1. In fact, using the arguments in the proof of Theorems 4.1 and 4.2, from any subsequence $\{u_{k_j}\}_{j \geq 0}$ of $\{u_k\}_{k \geq 0}$ we can extract another subsequence $\{u_{k_{j_m}}\}_{m \geq 0}$ converging in $W_0^{1,p}(\Omega)$ to some $\tilde{u}_\infty \in V_\infty$ satisfying $\mu_\infty = \mathcal{J}(\tilde{u}_\infty)$.

4.2 Auxiliary Result

Let $\{\mathcal{T}_k\}_{k \geq 0}$ be the triangulation sequence generated by Algorithm 1. First, we introduce the following notation,

$$\mathcal{T}_k^+ := \bigcap_{\ell \geq k} \mathcal{T}_\ell, \quad \mathcal{T}_k^0 := \mathcal{T}_k \setminus \mathcal{T}_k^+, \quad \Omega_k^+ := \bigcup_{T \in \mathcal{T}_k^+} D_T, \quad \Omega_k^0 := \bigcup_{T \in \mathcal{T}_k^0} D_T.$$

By definition, \mathcal{T}_k^+ consists of all elements not refined after the k -th iteration and any element in \mathcal{T}_k^0 are refined at least once after the k -th iteration. Note that $\mathcal{T}_\ell^+ \subset \mathcal{T}_k^+ \subset \mathcal{T}_k$ for $\ell < k$.

Next, we define a mesh-size function $h_k : \Omega \rightarrow \mathbb{R}^+$ almost everywhere by $h_k(x) = h_T$ for x in the interior of an element $T \in \mathcal{T}_k$ and $h_k(x) = h_F$ for x in the relative interior of face $F \in \mathcal{F}_k(\Omega)$. This mesh-size function has the following property [52],

$$\lim_{k \rightarrow \infty} \|h_k \chi_k^0\|_{L^\infty(\Omega)} = 0, \quad (4.10)$$

where χ_k^0 is the characteristic function of Ω_k^0 . Note that the uniform refinement strategy corresponds to $\|h_k\|_{L^\infty(\Omega)} \rightarrow 0$ as $k \rightarrow \infty$, and the resulting sequences of nested spaces satisfies $W_0^{1,p}(\Omega) = \overline{\bigcup_{k \geq 0} V_k}$.

Lemma 4.1. *Let $\{(\mu_{k_j}, u_{k_j})\}_{j \geq 0}$ be the convergent subsequence defined in Theorem 4.2 and let $\{\mathcal{M}_{k_j}\}_{j \geq 0}$ be the associate sequence of marked element patches, then there holds*

$$\lim_{j \rightarrow \infty} \max_{T \in \mathcal{M}_{k_j}} \eta_{k_j}(\mu_{k_j}, u_{k_j}; T) = 0. \quad (4.11)$$

Proof. Let $T_j \in \mathcal{M}_{k_j}$ be the element with the largest error indicator over \mathcal{M}_{k_j} for each k_j . As $\mathcal{M}_{k_j} \subset \mathcal{T}_{k_j}^0$, it is not difficult to know from (4.10) that

$$\begin{aligned} h_{T_j} &\leq \|h_{k_j} \chi_{k_j}^0\|_{L^\infty(\Omega)} \rightarrow 0 & \text{as } j \rightarrow \infty, \\ |T_j| \leq |D_{T_j}| &\leq C \|h_{k_j} \chi_{k_j}^0\|_{L^\infty(\Omega)}^d \rightarrow 0 & \text{as } j \rightarrow \infty. \end{aligned} \quad (4.12)$$

By virtue of (3.3) in Lemma 3.1, we have

$$\begin{aligned} \eta_{k_j}^q(\mu_{k_j}, u_{k_j}; T_j) &\leq C(h_{T_j}^q \|u_{k_j}\|_{L^p(T_j)}^p + \|\nabla u_{k_j}\|_{L^p(D_{T_j})}^p) \\ &\leq C\left(\|u_{k_j} - u_\infty\|_{L^p(\Omega)}^p + \|u_\infty\|_{L^p(T_j)}^p + \|\nabla(u_{k_j} - u_\infty)\|_{L^p(\Omega)}^p + \|\nabla u_\infty\|_{L^p(D_{T_j})}^p\right). \end{aligned}$$

Therefore, the desired vanishing limit comes from (4.12), (4.8) in Theorem 4.2 and the absolute continuity of $\|\cdot\|_{L^p(\Omega)}$ with respect to the Lebesgue measure. \square

Next, we introduce the residual with respect to the eigenpair (μ_k, u_k) ,

$$\langle \mathcal{R}(\mu_k, u_k), v \rangle := \int_{\Omega} |\nabla u_k|^{p-2} \nabla u_k \cdot \nabla v dx - \mu_k \int_{\Omega} |u_k|^{p-2} u_k v dx \quad \forall v \in W_0^{1,p}(\Omega).$$

To establish the convergence of this residual, we need to first recall the nodal interpolation operator $I_j : W^{2,\infty}(\Omega) \cap W_0^{1,p}(\Omega) \rightarrow V_j$ and the Scott-Zhang quasi-interpolation $\tilde{I}_j : W_0^{1,p}(\Omega) \rightarrow V_j$, which have the following approximation properties [27, 54],

$$\|\nabla(v - I_j v)\|_{L^p(T)} \leq C h_T^{1+d/p} |v|_{W^{2,\infty}(T)} \quad \forall T \in \mathcal{T}_j, \quad (4.13)$$

$$\|v - \tilde{I}_j v\|_{L^p(T)} + \sum_{F \in \partial T \cap \Omega} h_F^{1/p} \|v - \tilde{I}_j v\|_{L^p(F)} \leq C h_T \|\nabla v\|_{L^p(D_T)} \quad \forall T \in \mathcal{T}_j. \quad (4.14)$$

Lemma 4.2. *Let $\{(\mu_{k_j}, u_{k_j})\}_{j \geq 0}$ be the convergent subsequence defined in Theorem 4.2, there holds*

$$\lim_{j \rightarrow \infty} \langle \mathcal{R}(\mu_{k_j}, u_{k_j}), v \rangle = 0 \quad \forall v \in C_0^\infty(\Omega). \quad (4.15)$$

Proof. For the sake of brevity, k_j is abbreviated to j . For any $v \in C_0^\infty(\Omega)$, invoking the nodal interpolation operator I_j and the Scott-Zhang quasi-interpolation \tilde{I}_j associated with V_j , and noting the eigenpair (μ_j, u_j) satisfies (2.3) over \mathcal{T}_j , we derive

$$|\langle \mathcal{R}(\mu_j, u_j), v \rangle| = |\langle \mathcal{R}(\mu_j, u_j), v - I_j v \rangle| = \left| \langle \mathcal{R}(\mu_j, u_j), w - \tilde{I}_j w \rangle \right|.$$

Here, we denote $w := v - I_j v$. Combined with the elementwise integration by parts and Hölder inequality, this leads to

$$\begin{aligned} |\langle \mathcal{R}(\mu_j, u_j), v \rangle| &= \left| - \sum_{T \in \mathcal{T}_j} \int_T R_T(\mu_j, u_j)(w - \tilde{I}_j w) dx - \sum_{F \in \mathcal{F}_j(\Omega)} \int_F J_F(u_j)(w - \tilde{I}_j w) ds \right| \\ &\leq \sum_{T \in \mathcal{T}_j} \|R_T(\mu_j, u_j)\|_{L^q(T)} \|w - \tilde{I}_j w\|_{L^p(T)} + \sum_{F \in \mathcal{F}_j(\Omega)} \|J_F(u_j)\|_{L^q(F)} \|w - \tilde{I}_j w\|_{L^p(F)}. \end{aligned}$$

We further proceed by the error estimate (4.14), $\frac{1}{p} + \frac{1}{q} = 1$ and a split of \mathcal{T}_j into \mathcal{T}_ℓ^+ and $\mathcal{T}_j \setminus \mathcal{T}_\ell^+$ for some $\ell < j$ to find

$$\begin{aligned} |\langle \mathcal{R}(\mu_j, u_j), v \rangle| &\leq C \sum_{T \in \mathcal{T}_j} \left(h_T \|R_T(\mu_j, u_j)\|_{L^q(T)} \|\nabla w\|_{L^p(D_T)} + \sum_{F \subset \partial T \cap \Omega} h_F^{1/q} \|J_F(u_j)\|_{L^q(F)} \|\nabla w\|_{L^p(D_T)} \right) \\ &\leq C \sum_{T \in \mathcal{T}_j} \eta_j(\mu_j, u_j; T) \|\nabla(v - I_j v)\|_{L^p(D_T)} \\ &\leq C \left(\eta_j(\mu_j, u_j; \mathcal{T}_j \setminus \mathcal{T}_\ell^+) \|\nabla(v - I_j v)\|_{L^p(\Omega_\ell^0)} + \eta_j(\mu_j, u_j; \mathcal{T}_\ell^+) \|\nabla(v - I_j v)\|_{L^p(\Omega_\ell^+)} \right). \end{aligned}$$

With $\mathcal{T}_j(\Omega_\ell^0)$ denoting the restriction of \mathcal{T}_j over Ω_ℓ^0 , the error estimate for I_j (4.13) and the fact $|T| = h_T^d$ for any $T \in \mathcal{T}_j$ imply that for any $v \in C_0^\infty(\Omega)$,

$$\begin{aligned} \|\nabla(v - I_j v)\|_{L^p(\Omega_\ell^0)}^p &\leq C \sum_{T \in \mathcal{T}_j(\Omega_\ell^0)} h_T^{p+d} |v|_{W^{2,\infty}(T)}^p \leq C |\Omega| \|h_j\|_{L^\infty(\Omega_\ell^0)}^p \|v\|_{W^{2,\infty}(\Omega)}^p, \\ \|\nabla(v - I_j v)\|_{L^p(\Omega_\ell^+)}^p &\leq C \sum_{T \in \mathcal{T}_j} h_T^{p+d} |v|_{W^{2,\infty}(T)}^p \leq C \|v\|_{W^{2,\infty}(\Omega)}^p. \end{aligned}$$

Therefore, by the stability estimate (3.3) we arrive at

$$|\langle \mathcal{R}(\mu_j, u_j), v \rangle| \leq C_1 \|h_j\|_{L^\infty(\Omega_\ell^0)} \|v\|_{W^{2,\infty}(\Omega)} + C_2 \eta_j(\mu_j, u_j; \mathcal{T}_\ell^+) \|v\|_{W^{2,\infty}(\Omega)} \quad \forall v \in C_0^\infty(\Omega). \quad (4.16)$$

Let $\ell \rightarrow \infty$, then the first term on the right hand side of (4.16) goes to zero due to the monotonicity $h_j \leq h_\ell$ and (4.10).

To estimate the second term, the marking assumption (3.2) in Algorithm 1, combined with the fact $\mathcal{T}_\ell^+ \subset \mathcal{T}_j^+ \subset \mathcal{T}_j$ for $j > \ell$, leads to

$$\begin{aligned} \eta_j(\mu_j, u_j; \mathcal{T}_\ell^+) &\leq (\#\mathcal{T}_\ell^+)^{1/q} \max_{T \in \mathcal{T}_\ell^+} \eta_j(\mu_j, u_j; T) \\ &\leq (\#\mathcal{T}_\ell^+)^{1/q} \max_{T \in \mathcal{T}_j^+} \eta_j(\mu_j, u_j; T) \\ &\leq (\#\mathcal{T}_\ell^+)^{1/q} \max_{T \in \mathcal{M}_j} \eta_j(\mu_j, u_j; T), \end{aligned}$$

where $\#\mathcal{T}_\ell^+$ denotes the number of all elements in \mathcal{T}_ℓ^+ . Then Lemma 4.1 implies the second term tends to zero when $j \rightarrow \infty$. This proves the assertion. \square

Lemma 4.3. *Let $\{(\mu_{k_j}, u_{k_j})\}_{j \geq 0}$ be the convergent subsequence given by Theorem 4.2, then the following identity holds*

$$\lim_{j \rightarrow \infty} \langle \mathcal{R}(\mu_{k_j}, u_{k_j}), v \rangle = \int_{\Omega} |\nabla u_\infty|^{p-2} \nabla u_\infty \cdot \nabla v dx - \mu_\infty \int_{\Omega} |u_\infty|^{p-2} u_\infty v dx \quad \forall v \in W_0^{1,p}(\Omega). \quad (4.17)$$

Proof. We introduce two functionals $\mathcal{F}(v) := \int_{\Omega} |\nabla v|^p dx / p$ and $\mathcal{G}(v) := \int_{\Omega} |v|^p dx / p$ on $W_0^{1,p}(\Omega)$. As \mathcal{F} and \mathcal{G} are both C^1 functionals (cf. e.g. [8]) with

$$\begin{aligned} \mathcal{F}'(w)v &= \int_{\Omega} |\nabla w|^{p-2} \nabla w \cdot \nabla v dx, \\ \mathcal{G}'(w)v &= \int_{\Omega} |w|^{p-2} w v dx \quad \forall w, v \in W_0^{1,p}(\Omega). \end{aligned} \quad (4.18)$$

Theorem 4.2 leads to the desired assertion. \square

4.3 Main Result

Now we are in a position to state the main result of this paper.

Theorem 4.3. *Assume that the initial mesh \mathcal{T}_0 is sufficiently fine, i.e. $\|h_0\|_{L^\infty(\Omega)} \ll 1$. Let $\{(\mu_k, u_k)\}_{k \geq 0}$ be the sequence of discrete eigenpairs produced by Algorithm 1, then the following identities hold*

$$\begin{aligned} \lim_{k \rightarrow \infty} \mu_k &= \lambda_1, \\ \lim_{k \rightarrow \infty} \inf_{v \in E_{\lambda_1}} \|u_k - v\|_{W^{1,p}(\Omega)} &= 0. \end{aligned} \quad (4.19)$$

Proof. The proof is divided into three steps.

Step 1. By Theorem 4.2, $\mu_k \rightarrow \mu_\infty$ and there exists a subsequence $\{u_{k_j}\}$ such that $\|u_{k_j} - u_\infty\|_{W^{1,p}(\Omega)} \rightarrow 0$. First we prove that (μ_∞, u_∞) is an eigenpair of Problem (1.2). By the Hölder inequality and the stability estimate (3.4),

$$\begin{aligned} |\langle \mathcal{R}(\mu_k, u_k), v \rangle| &= \left| \int_{\Omega} |\nabla u_k|^{p-2} \nabla u_k \cdot \nabla v dx - \mu_k \int_{\Omega} |u_k|^{p-2} u_k v dx \right| \\ &\leq |u_k|_{W^{1,p}(\Omega)}^{p-1} \|v\|_{W^{1,p}(\Omega)} + \mu_k \|u_k\|_{L^p(\Omega)}^{p-1} \|v\|_{L^p(\Omega)} \\ &\leq C(\mu_0) \|v\|_{W^{1,p}(\Omega)} \quad \forall v \in W_0^{1,p}(\Omega). \end{aligned} \quad (4.20)$$

Hence, the sequence $\{\|\mathcal{R}(\mu_k, u_k)\|_{W^{-1,q}(\Omega)}\}_{k \geq 0}$ is uniformly bounded. This, together with Lemma 4.2 and the density of $C_0^\infty(\Omega)$ in $W_0^{1,p}(\Omega)$, implies that the convergent subsequence $\{(u_{k_j}, \mu_{k_j})\}_{j \geq 0}$ satisfies

$$\lim_{j \rightarrow \infty} \langle \mathcal{R}(\mu_{k_j}, u_{k_j}), v \rangle = 0 \quad \forall v \in W_0^{1,p}(\Omega).$$

In combination with Lemma 4.3, we derive

$$\int_{\Omega} |\nabla u_\infty|^{p-2} \nabla u_\infty \cdot \nabla v dx = \mu_\infty \int_{\Omega} |u_\infty|^{p-2} u_\infty v dx \quad \forall v \in W_0^{1,p}(\Omega). \quad (4.21)$$

This means that (μ_∞, u_∞) is an eigenpair of Problem (1.2).

Step 2. In view of (4.21) and Theorem 4.2, the first result in (4.19) is true once $\mu_\infty = \lambda_1$ is proved. To this end we define $E := \{u \in W_0^{1,p}(\Omega) \mid u \text{ satisfies (1.2) with } \|u\|_{L^p(\Omega)} = 1 \text{ for some } \lambda \in \mathbb{R}\}$, i.e. E consists of all $L^p(\Omega)$ -normalized eigenfunctions of Problem (1.2). Problem (1.2) has a nondecreasing sequence of positive eigenvalues tending to $+\infty$ [36, 46], so there holds $E_{\lambda_1} \subsetneq E$. Since any $u \in E_{\lambda_1}$ is a minimizer of \mathcal{J} over $W_0^{1,p}(\Omega)$, then we derive $\lambda_1 = \mathcal{J}(u) \leq \inf_{v \in E \setminus E_{\lambda_1}} \mathcal{J}(v)$. We prove by contradiction that the equality cannot happen. Let $\{w_n\}_{n \geq 0} \subset E \setminus E_{\lambda_1}$ be a minimizing sequence such that

$$\mathcal{J}(w_n) \rightarrow \inf_{v \in E \setminus E_{\lambda_1}} \mathcal{J}(v) = \lambda_1.$$

Then $\mathcal{J}(w_n)$ is a sequence of eigenvalues with λ_1 as its limit, contradicting the fact that λ_1 is isolated [47]. Thus, $\lambda_1 = \mathcal{J}(u) < \inf_{v \in E \setminus E_{\lambda_1}} \mathcal{J}(v)$ for any $u \in E_{\lambda_1}$.

Next, we justify the fineness condition on the initial mesh \mathcal{T}_0 in Algorithm 1. Assuming $\{\mathcal{T}_k\}_{k \geq 0}$ is a sequence of uniformly refined meshes, at this point $\|h_k\|_{L^\infty(\Omega)} \rightarrow 0$ and $W_0^{1,p}(\Omega) = \bigcup_{k \geq 0} \bar{V}_k$ as mentioned in Section 4.2. Therefore, for any $u \in E_{\lambda_1}$ there exists a sequence $\{v_\ell\}_{\ell \geq 0}$ with each $v_\ell \in \bar{V}_\ell$ such that $v_\ell \rightarrow u$ strongly in $W_0^{1,p}(\Omega)$. Noting \mathcal{J} is continuous over $W_0^{1,p}(\Omega)$ and $\mathcal{J}(u) = \lambda_1 < \inf_{v \in E \setminus E_{\lambda_1}} \mathcal{J}(v)$, we have $\mathcal{J}(v_\ell) < \inf_{v \in E \setminus E_{\lambda_1}} \mathcal{J}(v)$ for sufficiently large ℓ or sufficiently small mesh-size $\|h_\ell\|_{L^\infty(\Omega)}$. This observation and Theorem 4.2 imply that for the sequence of adaptively

generated meshes $\{\mathcal{T}_k\}_{k \geq 0}$ by Algorithm 1, we may choose a fine enough initial mesh \mathcal{T}_0 , over which there holds

$$\mathcal{J}(u_\infty) \leq \mathcal{J}(u_0) < \inf_{v \in E \setminus E_{\lambda_1}} \mathcal{J}(v). \quad (4.22)$$

On the other hand, by (4.21) in Step 1, $u_\infty \in E$. If $u_\infty \notin E_{\lambda_1}$, then $\mathcal{J}(u_\infty) \geq \inf_{v \in E \setminus E_{\lambda_1}} \mathcal{J}(v)$ and (4.22) yields an obvious contradiction. Therefore, $u_\infty \in E_{\lambda_1}$ and $\mu_\infty = \mathcal{J}(u_\infty) = \lambda_1$.

Step 3. To prove the second result in (4.19), we also proceed with mathematical contradiction. If the result is false, there exist a number $\varepsilon > 0$ and a subsequence $\{u_{k_j}\}_{j \geq 0}$ of $\{u_k\}_{k \geq 0}$ such that

$$\inf_{v \in E_{\lambda_1}} \|u_{k_j} - v\|_{W^{1,p}(\Omega)} \geq \varepsilon \quad \text{for all } k_j.$$

As discussed in Remark 4.1, we may extract another subsequence of $\{u_{k_{j_m}}\}_{m \geq 0}$ converging to some $\tilde{u} \in V_\infty$. Using the argument in Step 1 and the first result in (4.19), we further know that \tilde{u} satisfies (4.21) with $\mu_\infty = \lambda_1$, i.e. $\tilde{u} \in E_{\lambda_1}$. This is a contradiction. \square

5 Numerical Examples

To demonstrate the performance of Algorithm 1, we consider three 2-d numerical tests with a unit disk, a unit square and a L-shaped domain and three 3-d numerical examples with a unit cube, a 3-d L-shaped domain and a torus as the computational domain respectively in this section. All experiments are implemented in MATLAB R2020a on a personal computer with a 13th Gen Intel(R) Core(TM) i7-13700 (24 CPUs) and 32GB RAM, while the Partial Differential Equation Toolbox and the MATLAB package *iFEM* [26] are used in numerical simulations of 2-d and 3-d examples, respectively.

We utilize a normalized inverse iteration of sublinear supersolutions (IISS) [10, Algorithm 2] to solve Problem (2.1) over each mesh level, which is repeated in Algorithm 2 for the sake of completeness. Note that Algorithm 2 involves solving a p -Laplacian problem for the torsion function

Algorithm 2: Normalized IISS [10, Algorithm 2]

1: Solve (*torsion function*)

$$\begin{cases} -\Delta_p u_0 := -\nabla \cdot (|\nabla u_0|^{p-2} \nabla u_0) = 1 & \text{in } \Omega \\ u_0 = 0 & \text{on } \partial\Omega. \end{cases}$$

2: $m \leftarrow 0$.

3: $\lambda_m = 1/\|u_m\|_{L^\infty(\Omega)}^{p-1}$.

4: **do**

5: $m \leftarrow m + 1$.

6: Solve (*inverse iteration*)

$$\begin{cases} -\Delta_p u_m = (u_{m-1}/\|u_{m-1}\|_{L^\infty(\Omega)})^{p-1} & \text{in } \Omega, \\ u_m = 0 & \text{on } \partial\Omega. \end{cases}$$

7: $\lambda_m = 1/\|u_m\|_{L^\infty(\Omega)}^{p-1}$.

8: **while** $|\lambda_m - \lambda_{m-1}|/|\lambda_{m-1}| \geq \epsilon_M$

9: Return λ_m and $u_m/\|u_m\|_{L^\infty(\Omega)}$. (*first eigenvalue and first eigenfunction*)

in Step 1 and the inverse iteration sequence in Step 6. To do so, we call a decomposition coordination algorithm [4] as presented in Algorithm 3 with f being the right hand side of the p -Laplacian problem in Steps 1 and 6 of Algorithm 2 and $g = 0$ in the current situation.

Algorithm 3: Decomposition Coordination [4]

- 1: Define two vector fields $\xi_1, \nu_0: \Omega \rightarrow \mathbb{R}^d$; $n \leftarrow 0$.
- 2: **do**
- 3: $n \leftarrow n + 1$.
- 4: Compute u_n by solving a linear problem

$$\begin{cases} -\Delta u_n = \nabla \cdot (\xi_n - \nu_{n-1}) + f & \text{in } \Omega, \\ u_n = g & \text{on } \partial\Omega. \end{cases}$$

- 5: Compute ν_n by solving the algebraic nonlinear equation $|\nu_n|^{p-2} \nu_n + \nu_n = \xi_n + \nabla u_n$.
 - 6: Compute ξ_{n+1} as $\xi_{n+1} = \xi_n + \nabla u_n - \nu_n$.
 - 7: **while** $n = 1$ or $\frac{\|u_n - u_{n-1}\|_{L^2(\Omega)}}{\|u_{n-1}\|_{L^2(\Omega)}} > \epsilon_N$
 - 8: Return u_n .
-

In all experiments, the module MARK of Algorithm 1, utilizing Dörfler's strategy with $\theta = 0.6$ for the 2-d examples and $\theta = 0.8$ for the 3-d examples, yields a subset \mathcal{M}_k such that $\eta_k(\mu_k, u_k, \mathcal{M}_k) \geq \theta \eta_k(\mu_k, u_k)$. Algorithm 1 proceeds until the relative error for two consecutive approximate eigenvalues is below a prescribed tolerance ϵ_K , i.e. $|\mu_{k-1} - \mu_k|/\mu_{k-1} < \epsilon_K$. For large p in the 2-d examples and all p in the 3-d examples, an upper bound K is specified for the counter k of adaptive refinement steps. In Algorithm 3, we fix tolerance $\epsilon_N = 10^{-5}$, and each component of ξ_1 and ν_0 is an independent sample following the uniform distribution $U(0, 0.5)$. Figures 1-2 display all initial meshes used in Examples 5.1-5.6.

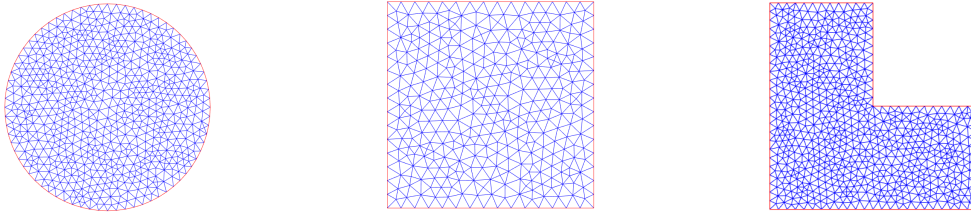


Figure 1: Initial meshes ($k = 0$ for \mathcal{T}_0) with the number of vertices being 682, 365, and 741 for Examples 5.1-5.3 from left to right.

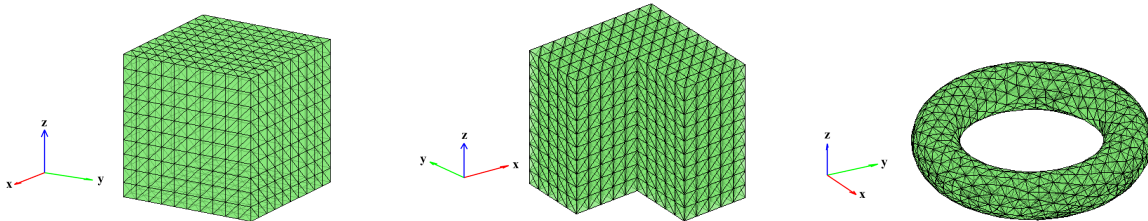


Figure 2: Initial meshes ($k = 0$ for \mathcal{T}_0) with the number of vertices being 1331, 585, and 959 for Examples 5.4-5.6 from left to right.

Example 5.1 (Unit Disk). In the first example, the computational domain is a unit disk centered at the origin. Numerical experiments are implemented for 9 different values of

$$p \in \{1.1, 1.5, 2, 2.5, 3, 4, 10, 20, 30\}.$$

Tolerance ϵ_K in Algorithm 1 is set to be 5×10^{-4} for $p = 4$ and 10^{-4} for the rest cases, among which the adaptive algorithm terminates if the counter $k > K = 9$ for $p = 10, 20, 30$, while tolerance ϵ_M in Algorithm 2 is 5×10^{-4} for $p = 1.1$, 10^{-5} for $p = 1.5, 2, 2.5$ and 5×10^{-5} for the rest.

For each p , approximate values, over meshes generated by the adaptive strategy, of the first eigenvalue of Problem (1.1) are provided in Table 1 ($p = 1.1, 1.5, 2, 2.5, 3$) and Table 2 ($p = 4, 10, 20, 30$) respectively, where k stands for the iteration number in Algorithm 1 while μ_k represents the approximate first eigenvalue over the k -th adaptive mesh. The results computed on fine meshes are listed in the last row as reference solutions. We observe that the sequence of computed eigenvalues $\{\mu_k\}_{k \geq 0}$ is decreasing and approaches the reference solution for each p as the adaptive mesh refinement level k increases. This numerical observation confirms the convergence of Algorithm 1 as proved in Theorem 4.3. As a benchmark, the first eigenvalue of Laplacian ($p = 2$) on the unit disk is approximately 5.78321. Our adaptive eigenvalue $\mu_7 = 5.78402$ as listed in the fifth column ($p = 2$) of Table 1 attains a 0.014% relative precision. One sees from Table 2 that the approximate eigenvalue $\mu_7 = 14.6713$ for $p = 4$ is smaller than the reference solution produced on a very fine mesh, which implies more accuracy with fewer degrees of freedom of Algorithm 1.

Figures 3-5 depict a selection of adaptive meshes generated by Algorithm 1 and computed first eigenfunctions over the finest adaptive meshes. For comparison, computed first eigenfunctions over very fine meshes are displayed in the last column of Figures 3 and 5. We observe that as p becomes larger, local refinements are performed in the vicinity of the origin. Moreover, as can be seen from the penultimate column of Figure 3 (Figures 3c-3k), the last column of Figure 4 (Figures 4d-4l) and the penultimate column of Figure 5 (Figures 5c-5k), the asymptotic behaviour of adaptively computed first eigenfunctions confirms two assertions in [42] and [41] that the first $L^\infty(\Omega)$ -normalized eigenfunction of (1.1) converges to 1, the characteristic function of the unit ball, as $p \rightarrow 1^+$ and to the distance function to the boundary, $1 - \sqrt{x_1^2 + x_2^2}$, as $p \rightarrow \infty$ respectively. This also explains the transition of additional mesh refinements from the whole domain to the center.

Table 1: Quantitative result for $p \in \{1.1, 1.5, 2, 2.5, 3\}$ in Example 5.1: the number of adaptive loops, the number of vertices and the computed first eigenvalue.

k	$p = 1.1$		$p = 1.5$		$p = 2$		$p = 2.5$		$p = 3$	
	vertices	μ_k	vertices	μ_k	vertices	μ_k	vertices	μ_k	vertices	μ_k
0	682	2.57807	682	4.02918	682	5.80632	682	7.75284	682	9.90463
1	1055	2.57749	1213	4.02732	1196	5.80145	1180	7.74343	2214	9.89018
2	1637	2.57671	2188	4.02431	2091	5.79601	2052	7.73324	1972	9.86859
3	2498	2.57662	3927	4.02137	3721	5.79006	3576	7.72451	3347	9.85650
4			6935	4.01992	6532	5.78718	6236	7.71776	5798	9.85249
5			12469	4.01888	11639	5.78542	10850	7.71546	9946	9.84022
6			22277	4.01842	20538	5.78440	18843	7.71253	17036	9.83989
7			39173	4.01822	35714	5.78402	32569	7.71199		
reference	24505	2.56642	65130	4.01790	65130	5.78342	65130	7.71122	65130	9.83481

Example 5.2 (Unit Square). We next consider the first eigenpair of (1.1) in a unit square $(0, 1)^2$ with $p = 1.2, 1.5, 2, 2.5, 3, 4, 10, 20, 30$. In this example, tolerance ϵ_K in Algorithm 1 is chosen as

Table 2: Quantitative result for $p \in \{4, 10, 20, 30\}$ Example 5.1: the number of adaptive loops, the number of vertices and the computed first eigenvalue.

k	$p = 4$		$p = 10$		$p = 20$		$p = 30$	
	vertices	μ_k	vertices	μ_k	vertices	μ_k	vertices	μ_k
0	682	14.8676	682	65.5562	682	270.463	682	792.061
1	1096	14.8350	936	64.0533	942	246.373	909	646.565
2	1838	17.7682	1400	62.6093	1269	224.980	1260	538.993
3	3041	14.7447	2184	62.0110	1854	218.470	1801	506.405
4	5179	14.7279	3460	61.7149	2765	210.819	2625	466.290
5	8820	14.7044	7935	61.4366	4210	207.801	3859	449.793
6	14818	14.6769	5577	61.1423	6515	205.064	5768	440.326
7	25078	14.6713	8991	60.8983	10146	203.304	8763	431.970
8			23717	60.8331	15968	202.576	13429	428.450
9			38698	60.6828	25387	201.803	20911	425.581
reference	86001	14.6833	76492	60.6684	76492	201.691	76492	423.168

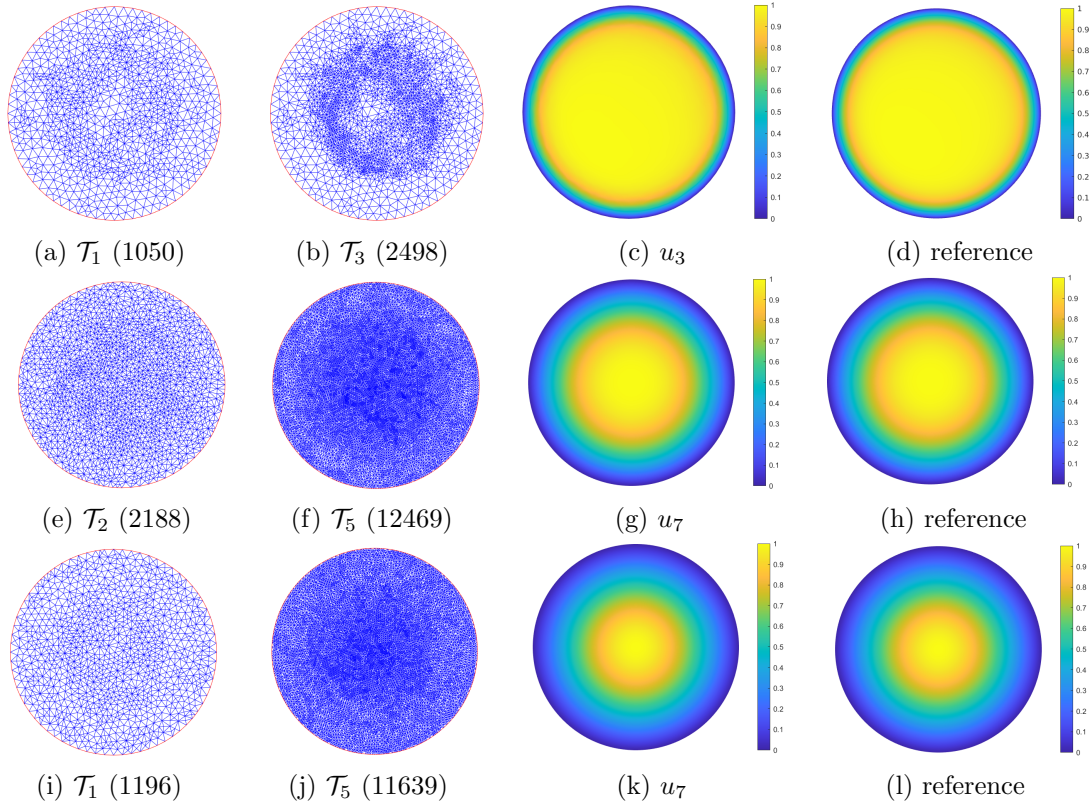


Figure 3: Adaptive mesh refinement level with the number of vertices over each mesh as well as final computed first eigenfunctions by adaptive refinements and references for $p = 1.1, 1.5, 2$ from top to bottom in Example 5.1.

5×10^{-4} for $p = 3$ and 10^{-4} for the rest p with a maximum adaptive refinement number $K = 9$ and $K = 10$ imposed for $p = 10, 20$ and $p = 30$ respectively while $\epsilon_M = 10^{-5}$ in Algorithm 2 except

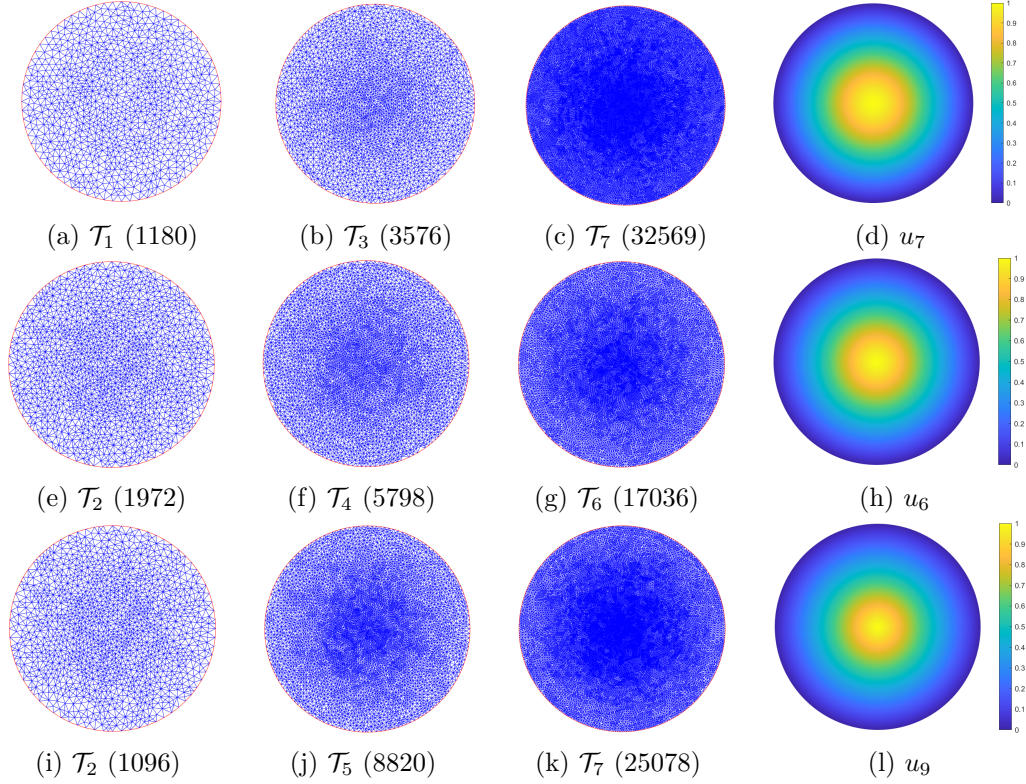


Figure 4: Adaptive mesh refinement level with the number of vertices over each mesh as well as final computed first eigenfunctions for $p = 2.5, 3, 4$ from top to bottom in Example 5.1.

for $p = 1.2$ and $p = 4$, in both of which $\epsilon_M = 5 \times 10^{-5}$.

Table 3 and Table 4 contain all computed first eigenvalues over adaptively generated meshes and very fine meshes as reference solutions. As in the previous example, the sequence of adaptive eigenvalues for each p strictly decreases to the reference solution. Noting that the exact first eigenvalue of Laplacian ($p = 2$) on the unit square is $2\pi^2 \approx 19.7392$, we see that our result $\mu_9 = 19.7410$ has an relative error less than 10^{-4} .

Sequences of adaptively generated meshes and computed first eigenfunctions over the final adaptive meshes as well as very fine meshes are displayed in Figures 6-8. The mesh is essentially refined in the vicinity of the center and around four corners as before for small p and then near two crossing diagonals for moderate $p > 2$. Finally, additional local refinements take place around the center for large p . This phenomenon is due to concentration of large gradients of numerical solutions as displayed in the penultimate column of Figure 6 (Figures 6c-6k), the last column of Figure 7 (Figures 7d-7l) and the penultimate column of Figure 8 (Figures 8c-8k). As stated in [42], the first eigenvalue of p -Laplacian converges to the Cheeger constant of Ω as $p \rightarrow 1^+$ and the characteristic function of the Cheeger domain is the associated eigenfunction of 1-Laplacian. In the current case $\Omega = (0, 1)^2$, the Cheeger domain is the unit square with each of its four corners rounded off by circular arcs of radius $1/(2 + \sqrt{\pi})$ [45, Theorem 3.9 and Remark 3.11]. The computed first eigenfunction in Figure 6c is obviously an approximation of the characteristic function of the relevant Cheeger domain. On the other hand, further inspection of Figures 8i-8j for $p = 30$ reveals that refinements are largely performed towards singularities in the vicinity of the center. The observation indirectly confirms the assertion in a recent paper [15] that the ∞ -ground state, as the limit of the first eigenfunction of p -Laplacian when $p \rightarrow \infty$, is ∞ -harmonic in the viscosity sense

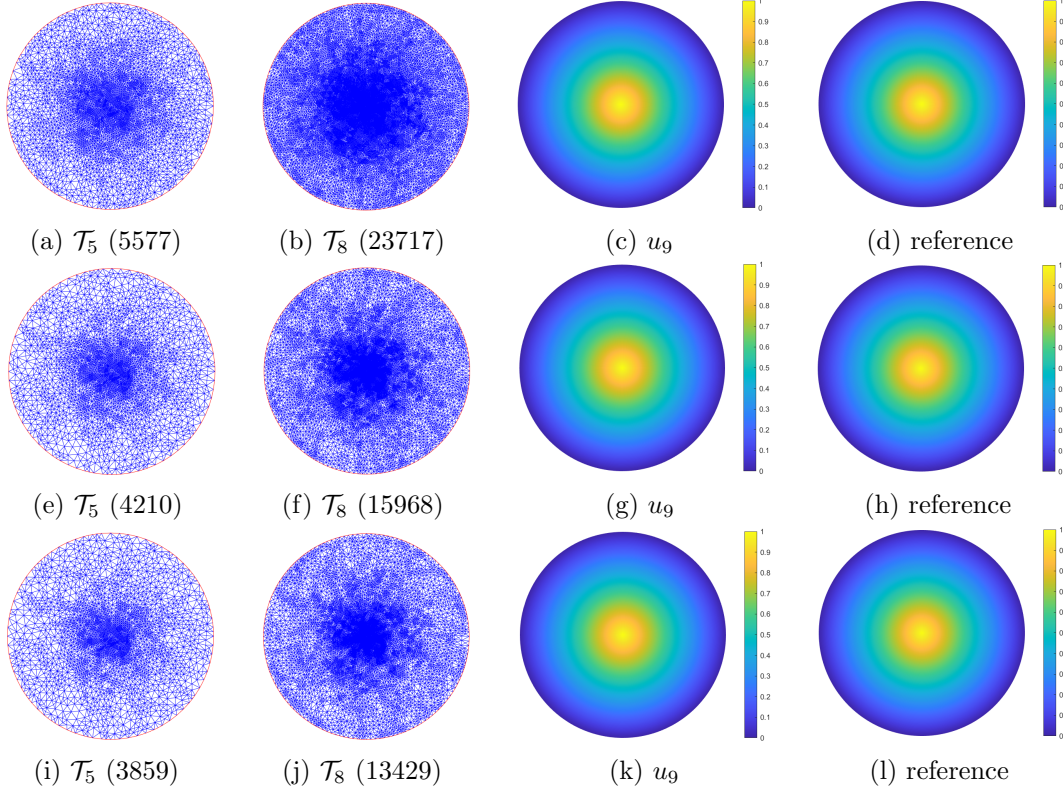


Figure 5: Adaptive mesh refinement level with the number of vertices over each mesh as well as final computed first eigenfunctions by adaptive refinements and references for $p = 10, 20, 30$ from top to bottom in Example 5.1.

and further continuously differentiable [53] in the unit square except on two diagonal segments lying in a symmetric neighbourhood around the center.

Table 3: Quantitative result for $p \in \{1.2, 1.5, 2, 2.5, 3\}$ in Example 5.2: the number of adaptive loops, the number of vertices and the computed first eigenvalue.

k	$p = 1.2$		$p = 1.5$		$p = 2$		$p = 2.5$		$p = 3$	
	vertices	μ_k	vertices	μ_k	vertices	μ_k	vertices	μ_k	vertices	μ_k
0	365	6.25529	365	10.1415	365	19.8951	365	36.3181	365	63.6013
1	590	6.23466	622	10.1186	637	19.8497	632	36.2091	629	63.3302
2	975	6.22154	1022	10.1038	1083	19.8148	1098	36.1092	1056	63.1296
3	1605	6.21414	1744	10.0929	1885	19.7843	1908	36.0469	1842	62.9704
4	2589	6.20896	2995	10.0840	3257	19.7670	3290	36.0087	3150	62.8610
5	4098	6.20632	5071	10.0791	5640	19.7552	5719	35.9825	5416	62.8523
6	6238	6.20505	8775	10.0764	9908	19.7484	9928	35.9697	9289	62.7673
7	9569	6.20475	15097	10.0745	17197	19.7445	16952	35.9584	15780	62.7476
8			26287	10.0735	29834	19.7424	28760	35.9533		
9					51244	19.7410	48867	35.9526		
reference	23972	6.19606	61431	10.0723	61431	19.7400	61431	35.9473	61431	62.7522

Example 5.3 (L-shaped Domain). The third example is posed in an L-shaped domain $(0, 2)^2 \setminus [1, 2]^2$

Table 4: Quantitative result for $p \in \{4, 10, 20, 30\}$ in Example 5.2: the number of adaptive loops, the number of vertices and the computed first eigenvalue.

k	$p = 4$		$p = 10$		$p = 20$		$p = 30$	
	vertices	μ_k	vertices	μ_k	vertices	μ_k	vertices	μ_k
0	365	180.480	365	4.01445×10^4	365	1.31523×10^8	365	3.32338×10^{11}
1	592	179.080	478	3.84212×10^4	459	1.14423×10^8	538	2.63117×10^{11}
2	1002	178.081	692	3.72617×10^4	613	1.04613×10^8	684	2.29447×10^{11}
3	1679	177.536	1055	3.68261×10^4	870	1.01255×10^8	905	2.04656×10^{11}
4	2849	177.190	1654	3.64416×10^4	1308	9.82599×10^7	1273	1.93808×10^{11}
5	4850	176.864	2693	3.62735×10^4	2006	9.67871×10^7	1810	1.84294×10^{11}
6	8108	176.849	4359	3.61551×10^4	3089	9.57319×10^7	2617	1.81342×10^{11}
7			7134	3.60413×10^4	4945	9.53923×10^7	3888	1.78707×10^{11}
8			11722	3.60351×10^4	7902	9.49911×10^7	5887	1.77028×10^{11}
9			19286	3.59512×10^4	12756	9.46224×10^7	9026	1.75533×10^{11}
10							14000	1.75363×10^{11}
reference	61431	176.750	69177	3.58589×10^4	69177	9.25536×10^7	69177	1.67213×10^{11}

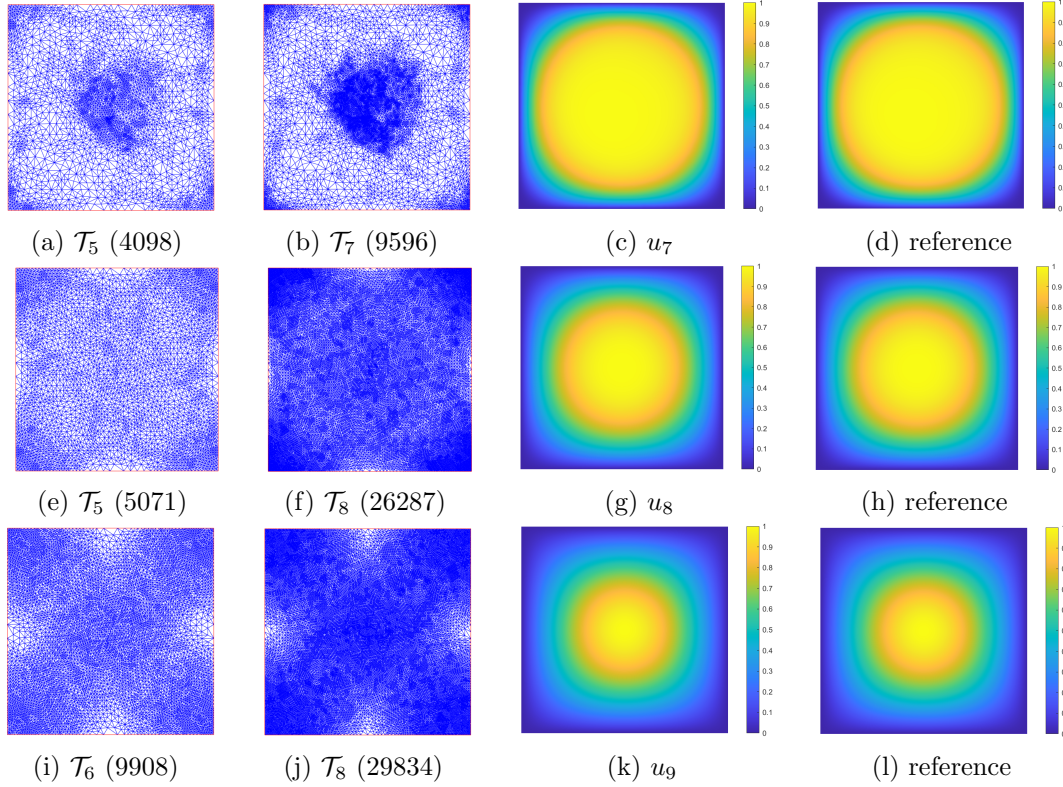


Figure 6: Adaptive mesh refinement level with the number of vertices over each mesh as well as final computed first eigenfunctions by adaptive refinements and references for $p = 1.2, 1.5, 2$ from top to bottom in Example 5.2.

with the same values of p as in Example 5.1. Tolerances ϵ_K and ϵ_M are given by 10^{-4} and 10^{-5} for $p \in \{1.5, 2, 2.5, 3\}$, 5×10^{-4} and 5×10^{-5} for $p \in \{4, 10, 20, 30\}$ and 10^{-3} and 5×10^{-4} for $p = 1.1$ respectively. A maximum iteration number is specified as $K = 9$ for $p = 10, 20$ and $K = 11$ for

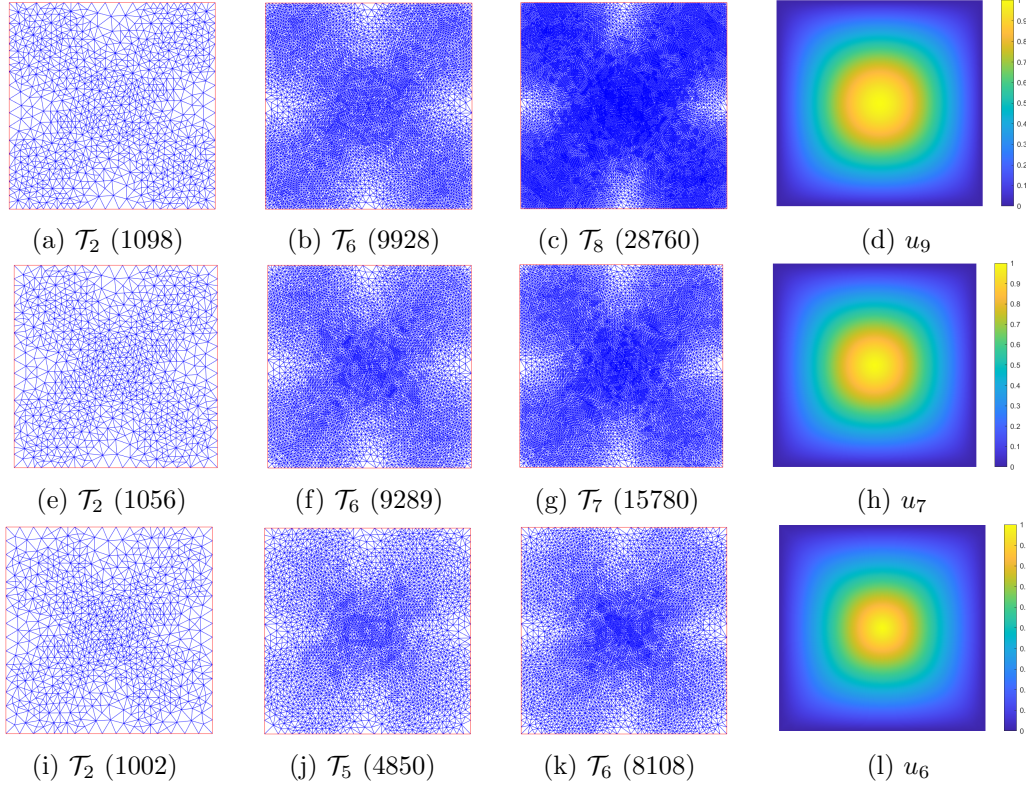


Figure 7: Adaptive mesh refinement level with the number of vertices over each mesh as well as final computed first eigenfunctions by adaptive refinements for $p = 2.5, 3, 4$ from top to bottom in Example 5.2.

$p = 30$ respectively.

The convergence history of Algorithm 1 is presented in Tables 5 and 6, which show similar convergence behaviour of computed first eigenvalues for each p . Compared with the reference solution over the fine mesh, fewer degrees of freedom by Algorithm 1 is required for more accuracy when p is small. In particular, we observe from Table 6 with $p = 4$ that the computed eigenvalues $\mu_{11} = 54.6221$ and $\mu_{12} = 54.6211$ by Algorithm 1, albeit with only 49% and 78% of degrees of freedom respectively, are both smaller than the reference solution over a very fine mesh.

Figures 9-11 show that the marked set from Algorithm 1 transfers from the region adjacent to the six corners to the vicinity of $(\frac{1}{2}, \frac{1}{2})$ and the area around the reentrant corner as p increases, and the singularities are clearly detected for each p . From the penultimate column of Figure 9 (Figures 9c-9g), we may deduce as in Example 5.2 that the computed first eigenfunctions are approximations of the characteristic function associated with some Cheeger domain [42] as the first eigenfunction of 1-Laplacian in Ω . In addition, it seems that singularities for large p might exist along the segment connecting $(\frac{1}{2}, \frac{1}{2})$ to $(1, 1)$ as displayed in Figure 11f. To the best of our knowledge, no reasonable explanation of this observation is available in the PDE theory. This might provide a clue about the regularity of the ∞ -eigenvalue problem in a non-convex domain.

Example 5.4 (Unit Cube). The first 3-d experiment is conducted in the unit cube $(0, 1)^3$ with 4 different values of $p \in \{1.5, 2, 4, 10\}$. Tolerance ϵ_M in Algorithm 2 is fixed at 10^{-5} . Due to the limited computing resource, a maximum adaptive refinement number K is prescribed instead of a tolerance ϵ_K for all p .

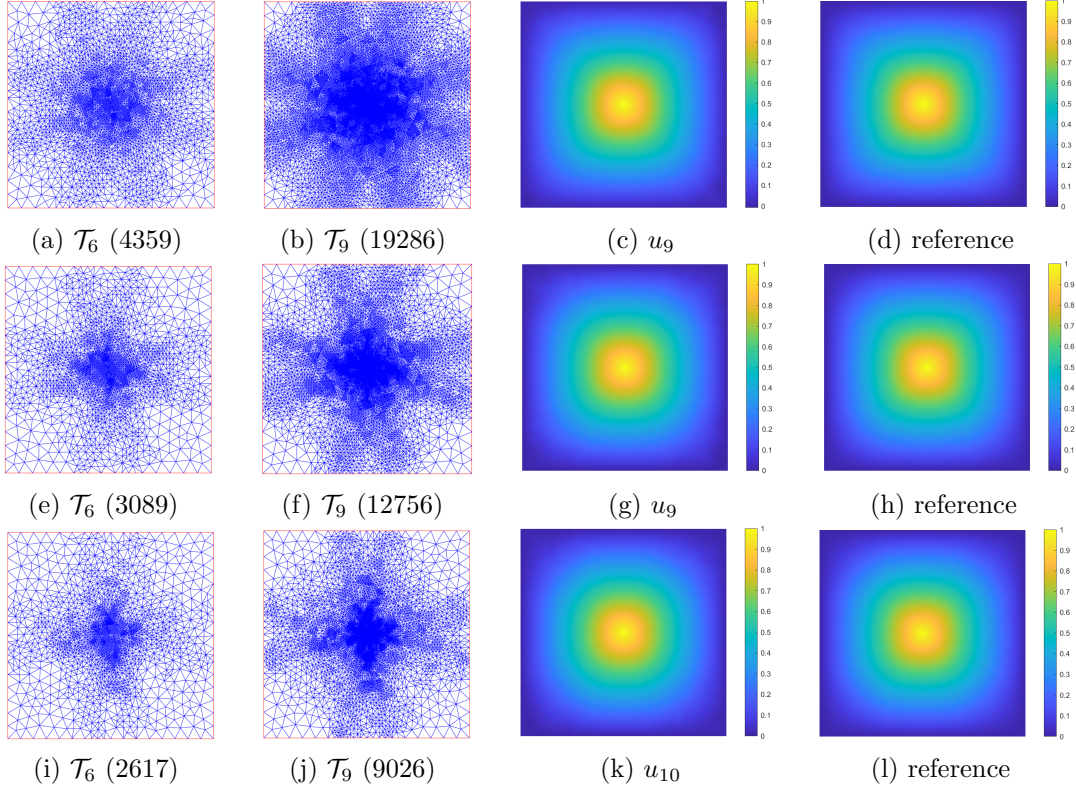


Figure 8: Adaptive mesh refinement level with the number of vertices over each mesh as well as final computed first eigenfunctions by adaptive refinements and references for $p = 10, 20, 30$ from top to bottom in Example 5.2.

Table 5: Quantitative result for $p \in \{1.1, 1.5, 2, 2.5, 3\}$ in Example 5.3: the number of adaptive loops, the number of vertices and the computed first eigenvalue.

k	$p = 1.1$		$p = 1.5$		$p = 2$		$p = 2.5$		$p = 3$	
	vertices	μ_k	vertices	μ_k	vertices	μ_k	vertices	μ_k	vertices	μ_k
0	741	3.29084	741	5.74153	741	9.75107	741	15.6646	741	24.4197
1	1240	3.27061	1245	5.71661	1188	9.70099	1111	15.5862	1064	24.2656
2	1994	3.26325	2121	5.70591	1990	9.68609	1766	15.5381	1606	24.1712
3	3286	3.25550	3643	5.69624	3385	9.66841	2903	15.5029	2556	24.1022
4	5246	3.25223	6245	5.69123	5748	9.65753	4856	15.4807	4193	24.0693
5	8394	3.24729	10657	5.68770	9842	9.65065	8119	15.4662	6889	24.0321
6	13325	3.24471	18444	5.68576	16767	9.64646	13653	15.4577	11378	24.0204
7			31828	5.68436	28561	9.64385	22892	15.4511	18715	24.0061
8			54608	5.68362	48554	9.64225	38111	15.4488	30495	24.0023
9			94803	5.68311	82874	9.64127	63517	15.4469	50007	23.9932
10					140675	9.64066	105876	15.4448	81801	23.9923
11							175649	15.4444		
reference	20390	3.24002	122801	5.683402	209247	9.64097	256870	15.4449	256870	23.9903

Table 7 presents the number of vertices and computed first eigenvalues over adaptively refined meshes. As shown in the previous 2-d numerical tests, the sequence of adaptive eigenvalues for each

Table 6: Quantitative result for $p \in \{4, 10, 20, 30\}$ in Example 5.3: the number of adaptive loops, the number of vertices and the computed first eigenvalue.

k	$p = 4$		$p = 10$		$p = 20$		$p = 30$	
	vertices	μ_k	vertices	μ_k	vertices	μ_k	vertices	μ_k
0	741	56.1189	741	4.31754×10^3	741	2.70810×10^6	741	1.30341×10^9
1	972	55.5998	848	4.15542×10^3	820	2.46503×10^6	813	1.11285×10^9
2	1384	55.2551	1016	4.01369×10^3	943	2.32909×10^6	907	9.12838×10^8
3	2087	55.0287	1296	3.93108×10^3	1144	2.12411×10^6	1053	8.74190×10^8
4	3267	54.8835	1762	3.88738×10^3	1418	2.04914×10^6	1267	7.94392×10^8
5	5144	54.7934	2483	3.85769×10^3	1839	1.99152×10^6	1616	7.60674×10^8
6	8215	54.7351	3553	3.84105×10^3	2477	1.97362×10^6	2153	7.43803×10^8
7	13142	54.6975	5245	3.82974×10^3	3491	1.95886×10^6	2952	7.33018×10^8
8	20845	54.6695	7862	3.82284×10^3	5047	1.94891×10^6	4229	7.24466×10^8
9	33364	54.6506	11912	3.81893×10^3	7444	1.94260×10^6	6180	7.22056×10^8
10	53165	54.6445					9148	7.19039×10^8
11	84384	54.6221					13697	7.17379×10^8
12	134431	54.6211						
reference	172212	54.6323	44439	3.81345×10^3	44439	1.92416×10^6	44439	7.03153×10^8

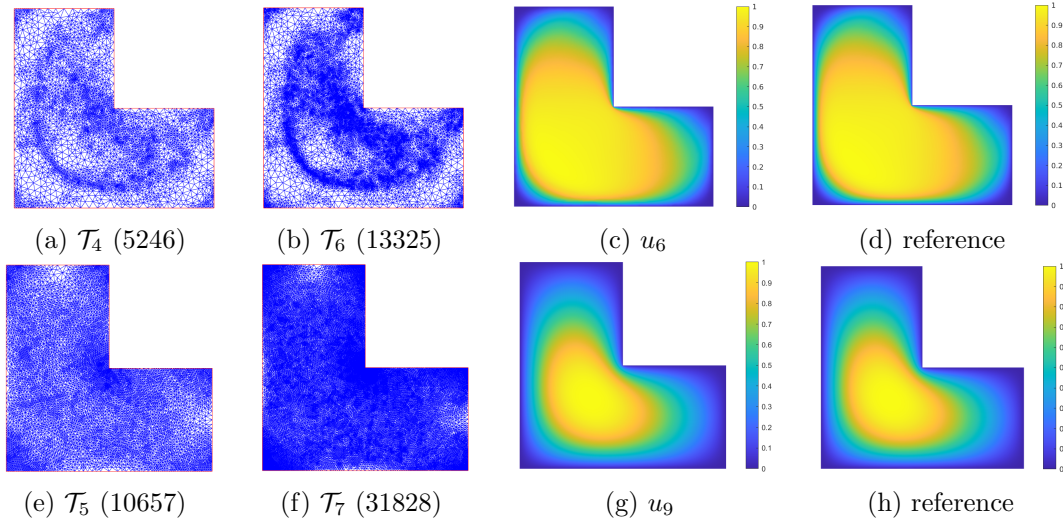


Figure 9: Adaptive mesh refinement level with the number of vertices over each mesh as well as final computed first eigenfunctions by adaptive refinements and references for $p = 1.1$ (1st row) and $p = 1.5$ (2nd row) in Example 5.3.

p monotonically decreases. It is worth mentioning that $\mu_9 = 29.6297$ for $p = 2$ attains an relative error about 7×10^{-4} with respect to the exact first eigenvalue $3\pi^2 \approx 29.6088$ of Laplacian in the unit cube. To illustrate the efficiency of Algorithm 1, the numerical simulation of $p = 2$ yields an approximate first eigenvalue 29.9918 over a fine mesh with 373248 vertices whereas our adaptive algorithm can achieve higher accuracy ($\mu_8 = 29.6456$) at a cost of almost half vertices (188348).

In Figure 12, we depict the evolution of adaptive meshes and computed first eigenfunctions over the finest adaptive meshes in the cross section $x < 0.5$ due to the symmetry. As in cases of the 2-d unit square, refinements are largely performed in the vicinity of the center and around four corners for small p and then in the region where the computed first eigenfunctions are non-zero for large p .

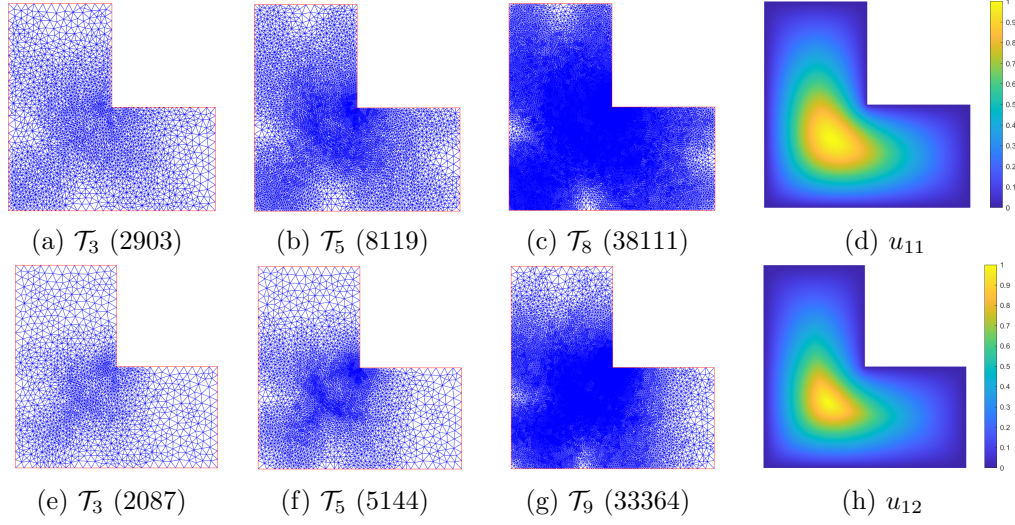


Figure 10: Adaptive mesh refinement level with the number of vertices over each mesh as well as final computed first eigenfunctions by adaptive refinements for $p = 2.5$ (1st row) and 4 (2nd row) in Example 5.3.

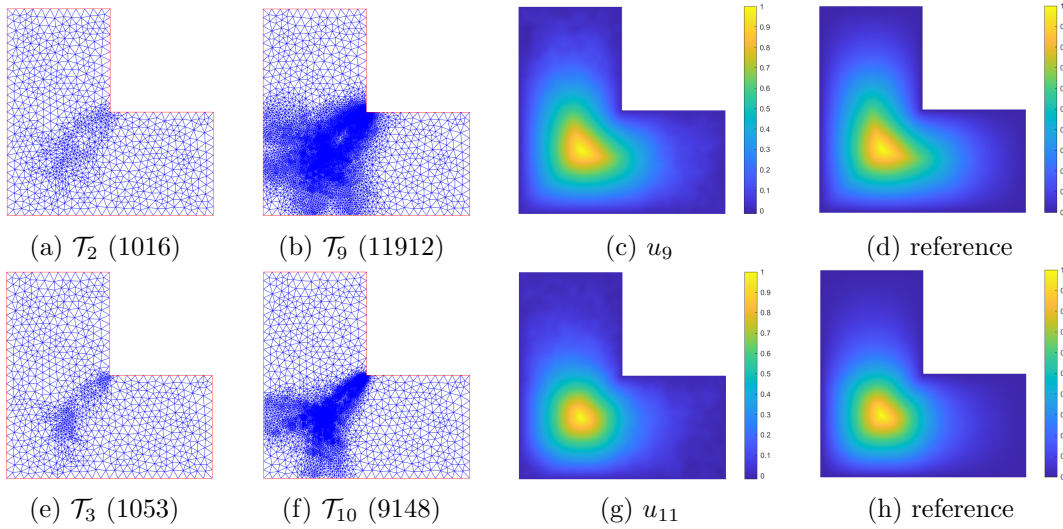


Figure 11: Adaptive mesh refinement level with the number of vertices over each mesh as well as final computed first eigenfunctions by adaptive refinements and references for $p = 10$ (1st row) and 30 (2nd row) in Example 5.3.

Example 5.5 (3-d L-shaped Domain). In this example we consider Problem (1.2) in a 3-d L-shaped domain $(0, 2)^3 \setminus (0, 1] \times (0, 1] \times (0, 2)$. The experiments are performed for 3 different values of $p \in \{1.5, 4, 10\}$. The parameter ϵ_M is set to be 10^{-5} and the number of loops K in Algorithm 1 is specified as in Table 8.

Computed first eigenvalues as well as associated numbers of vertices over adaptively generated meshes are listed in Table 8. As before, the sequence of numerical first eigenvalues demonstrates a steadily decreasing trend with the number of vertices increasing. A selection of adaptive meshes and the computed first eigenfunction over the finest adaptive mesh in the cross section $z < 1$ for each p are visualized in Figure 13 due to the symmetry. In the horizontal direction, we observe

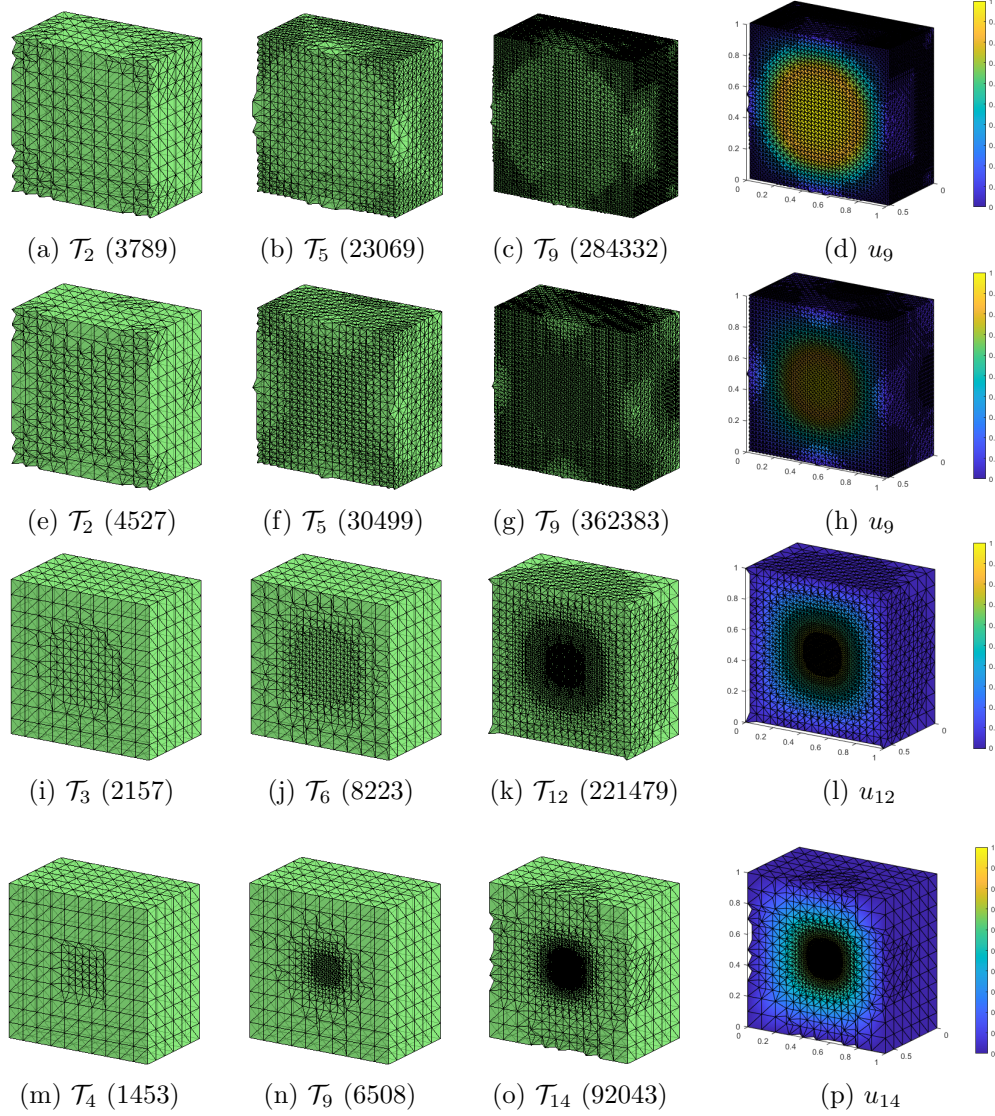


Figure 12: Adaptive mesh refinement level with the number of vertices over each mesh as well as final computed first eigenfunctions by adaptive refinements in the cross section $x < 0.5$ for $p = 1.5, 2, 4, 10$ from top to bottom in Example 5.4.

refinements near the six corners for small p and then evidently in the interior as well as adjacent to the reentrant corner for large p . This behaviour is similar to that in Example 5.3 for the 2-d case. In addition, local refinements occur vertically along the concave edge with strong singularities as p increases. However, the refined region shrinks as the computed first eigenfunction vanishes in the most part of Ω .

Example 5.6 (Torus). The computational domain of the last example is a torus with major radius 0.8 and minor radius 0.1 centered at the origin with $p = 2$ and $p = 4$. Due to the limited memory of the computer, a maximum number of refinement K is specified as in Table 9 and the tolerance ϵ_M is set to be 10^{-5} and 5×10^{-5} for $p = 2$ and $p = 4$ respectively. Table 9 documents the computed first eigenvalues featuring a gradually steady decline as the adaptive meshes evolves. Figure 14 displays the adaptive meshes generated by Algorithm 1 and visualize the computed first eigenfunctions over

Table 7: Quantitative result for $p \in \{1.5, 2, 4, 10\}$ in Example 5.4: the number of adaptive loops, the number of vertices and the computed first eigenvalue.

k	$p = 1.5$		$p = 2$		$p = 4$		$p = 10$	
	vertices	μ_k	vertices	μ_k	vertices	μ_k	vertices	μ_k
0	1331	14.9719	1331	30.8578	1331	346.595	1331	1.48342×10^5
1	2003	14.8508	2183	30.4664	1428	339.998	1341	1.32567×10^5
2	3789	14.6678	4527	29.9688	1713	333.102	1389	1.20605×10^5
3	7193	14.6143	7798	29.9302	2157	329.550	1453	1.18186×10^5
4	11871	14.5777	14095	29.8301	3049	323.672	1605	1.09896×10^5
5	23069	14.5361	30499	29.7193	5167	319.016	1810	1.06198×10^5
6	42768	14.5179	53979	29.6903	8223	315.660	2215	1.02281×10^5
7	76375	14.5053	92036	29.6710	13864	312.402	2899	9.91547×10^4
8	148519	14.4948	188348	29.6456	24899	310.919	4363	9.57893×10^4
9	284332	14.4892	362383	29.6297	41528	310.086	6508	9.21262×10^4
10					70878	309.285	10285	9.04754×10^4
11					128276	308.471	18264	8.77086×10^4
12					221479	307.792	30195	8.66154×10^4
13							51359	8.55563×10^4
14							92043	8.51059×10^4

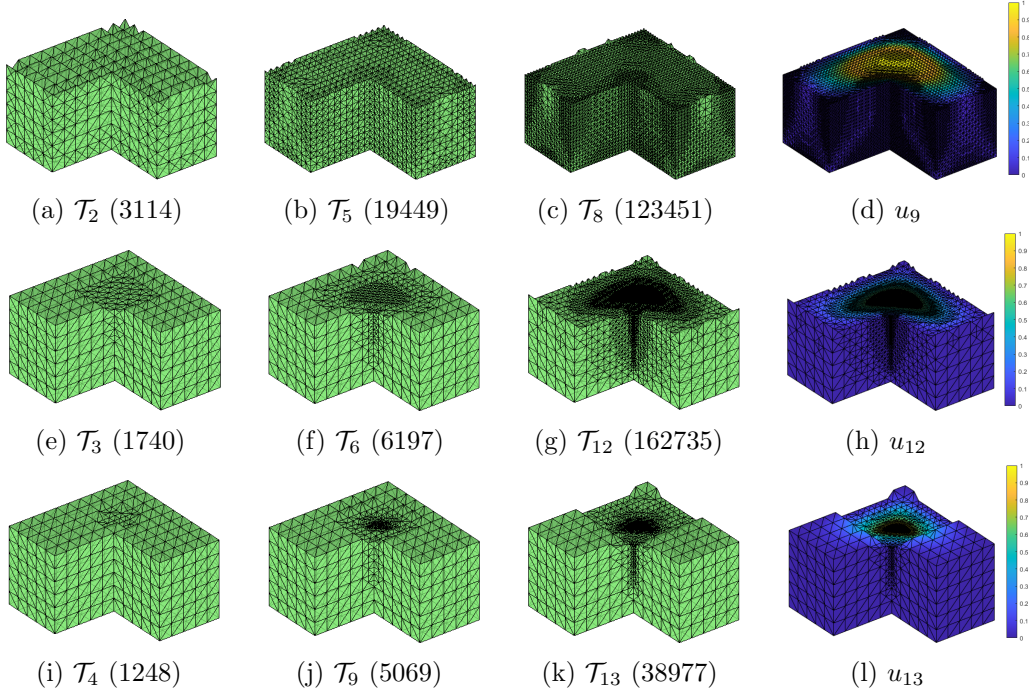


Figure 13: Adaptive mesh refinement level with the number of vertices over each mesh as well as final computed first eigenfunctions by adaptive refinements in the cross section $z < 1$ for Example 5.5: $p = 1.5, 4, 10$ from top to bottom.

the finest adaptive meshes in the cross section $z < 0$ due to the symmetry. As illustrated in Figure

Table 8: Quantitative result for $p \in \{1.5, 4, 10\}$ in Example 5.5: the number of adaptive loops, the number of vertices and the computed first eigenvalue.

k	$p = 1.5$		$p = 4$		$p = 10$	
	vertices	μ_k	vertices	μ_k	vertices	μ_k
0	1056	7.72402	1056	81.0511	1056	8.28107×10^3
1	1646	7.59132	1138	80.0312	1070	8.40531×10^3
2	3114	7.40312	1374	75.8082	1095	7.10282×10^3
3	5905	7.33215	1740	73.6532	1118	6.90217×10^3
4	9829	7.29308	2470	71.9343	1248	6.42960×10^3
5	19449	7.24515	4006	70.3522	1470	5.96310×10^3
6	36541	7.22480	6197	69.3535	1775	5.66794×10^3
7	63085	7.21281	18437	68.6378	2345	5.37915×10^3
8	123451	7.19806	24899	68.1258	3423	5.15780×10^3
9	231816	7.19169	30702	67.7104	5069	4.97964×10^3
10			52381	67.4119	8046	4.86127×10^3
11			95228	67.1837	14011	4.76670×10^3
12			162735	67.0321	22848	4.70221×10^3
13					38977	4.63375×10^3

14, the support of the first eigenfunction is shaped like a crescent and becomes narrower with larger p . This results in concentrated local refinements.

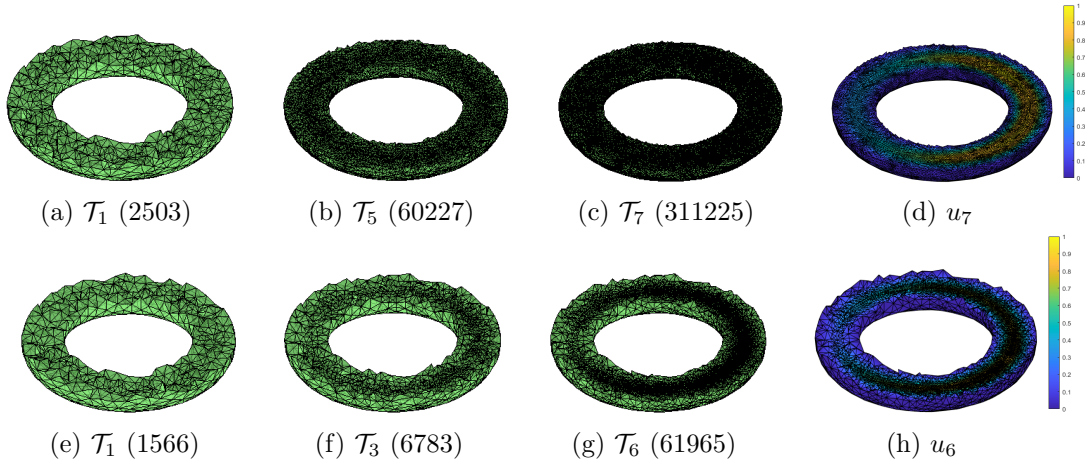


Figure 14: Adaptive mesh refinement level with the number of vertices over each mesh as well as final computed first eigenfunctions by adaptive refinements in the cross section $z < 0$ for $p = 2$ (1st row) and $p = 4$ (2nd row) in Example 5.6.

6 Conclusions

An adaptive finite element method has been designed to approximate the first eigenvalue of the p -Laplacian operator. We have proved that the sequence of discrete eigenvalues and discrete eigenfunctions converges to the exact one and the related eigenset respectively with the help of

Table 9: Quantitative result for $p \in \{2, 4\}$ in Example 5.6: the number of adaptive loops, the number of vertices and the computed first eigenvalue.

k	$p = 2$		$p = 4$	
	vertices	μ_k	vertices	μ_k
0	959	158.135	959	1.14221×10^4
1	2503	156.570	1566	1.12114×10^4
2	4824	154.365	3451	1.08483×10^4
3	11288	152.046	6783	1.04961×10^4
4	26008	150.206	13613	1.01963×10^4
5	60227	148.546	29387	9.94798×10^3
6	142157	146.881	61965	9.75105×10^3
7	311225	145.279		

minimization techniques in derivation of existence result for nonlinear elliptic equations. In the process, a residual-type error estimator is available and serves in the module ESTIMATE of the adaptive algorithm. The asymptotic behavior of computed first eigenfunctions shows that our adaptive algorithm can capture the singularities as described in the PDE theory. Since the conforming finite element method only provides an upper bound for the first eigenvalue, one natural question is how to yield a lower bound. One possible choice is the nonconforming finite element method, which works for 2-Laplacian [5, 20, 40, 50, 51, 59]. In view of this, our future research topic is the study of an adaptive nonconforming method for the first eigenpair of p -Laplacian.

Funding The research of Guanglian Li was partially supported by Hong Kong RGC through General Research Fund (project number: 17317122) and Early Career Scheme (project number: 27301921). The research of Yifeng Xu was partially supported by the National Natural Science Foundation of China (Projects 12250013, 12261160361 and 12271367), the Science and Technology Commission of Shanghai Municipality (Projects 20JC1413800 and 22ZR1445400) and General Research Fund (Projects KF202318 and KF202468) from Shanghai Normal University. The work of Shengfeng Zhu was partially supported by the National Key Basic Research Program under grant 2022YFA1004402, the National Natural Science Foundation of China (12471377), and the Science and Technology Commission of Shanghai Municipality (Projects 22ZR1421900 and 22DZ2229014).

References

- [1] R. Adams and J. Fournier, *Sobolev Spaces*, 2nd ed., Elsevier Science/Academic Press, Amsterdam, 2003.
- [2] M. Ainsworth and J. T. Oden, *A Posteriori Error Estimation in Finite Element Analysis*, Pure and Applied Mathematics, Wiley-Interscience, New York, 2000.
- [3] A. Ambrosetti and A. Malchiodi, *Nonlinear Analysis and Semilinear Elliptic Problems*, Cambridge University Press, Cambridge, 2007.
- [4] A. Aragón, J. Fernández Bonder and D. Rubio, *Effective numerical computation of $p(x)$ -Laplace equations in 2D*, Int. J. Comput. Math., 100 (2023), 2111-2123.

- [5] M. G. Armentano and R. G. Durán, *Asymptotic lower bounds for eigenvalues by nonconforming finite element methods*, Electron. Trans. Numer. Anal., 17 (2004), 93-101.
- [6] C. Atkinson and C. R. Champion, *Some boundary-value problems for the equation $\nabla \cdot (|\nabla\phi|^N \nabla\phi) = 0$* , Quart. J. Mech. Appl. Math., 37 (1984), 401-419.
- [7] I. Babuška and W. Rheinboldt, *Error estimates for adaptive finite element computations*, SIAM J. Numer. Anal., 15 (1978), 736-754.
- [8] M. Badiale and E. Serra, *Semilinear Elliptic Equations for Beginners*, Springer-Verlag, London, 2011.
- [9] L. Belenki, L. Diening and C. Kreuzer, *Optimality of an adaptive finite element method for the p -Laplacian equation*, IMA J. Numer. Anal., 32 (2012), 484-510.
- [10] R. J. Biezuner, J. Brown, G. Ercole and E. M. Martins, *Computing the first eigenpair of the p -Laplacian via inverse iteration of sublinear supersolutions*, J. Sci. Comput., 52 (2012), 180-201.
- [11] R. J. Biezuner, G. Ercole and E. M. Martins, *Computing the first eigenvalue of the p -Laplacian via the inverse power method*, J. Funct. Anal., 257 (2009), 243-270.
- [12] D. Boffi, D. Gallistl, F. Gardini and L. Gastaldi, *Optimal convergence of adaptive FEM for eigenvalue clusters in mixed form*, Math. Comp., 86 (2017), 2213-2237.
- [13] G. Bognár and T. Szabó, *Solving nonlinear eigenvalue problems by using p -version of FEM*, Comput. Math. Appl., 43 (2003), 57-68.
- [14] A. Bonito and A. Demlow, *Convergence and optimality of higher-order adaptive finite element methods for eigenvalue clusters*, SIAM J. Numer. Anal., 54 (2016), 2379-2388.
- [15] K. K. Brustad, E. Lindgren and P. Lindqvist, *The infinity-Laplacian in smooth convex domains and in a square*, Mathematics in Engineering, 5 (2023), 1-16.
- [16] C. Carstensen, M. Feischl, M. Page and D. Praetorius, *Axioms of adaptivity*, Comp. Math. Appl., 67 (2014), 1195-1253.
- [17] C. Carstensen, D. Gallistl and M. Schedensack, *Adaptive nonconforming Crouzeix-Raviart FEM for eigenvalue problems*, Math. Comp., 84 (2015), 1061-1087.
- [18] C. Carstensen and J. Gedicke, *An oscillation-free adaptive FEM for symmetric eigenvalue problems*, Numer. Math., 118 (2011), 401-427.
- [19] C. Carstensen and J. Gedicke, *An adaptive finite element eigenvalue solver of asymptotic quasi-optimal computational complexity*, SIAM J. Numer. Anal., 50 (2012), 1029-1057.
- [20] C. Carstensen and J. Gedicke, *Guaranteed lower bounds for eigenvalues*, Math. Comp., 83 (2014), 2605-2629.
- [21] C. Carstensen, W. Liu and N. Yan, *A posteriori FE error control for p -Laplacian by gradient recovery in quasi-norm*, Math. Comp., 75 (2006), 1599-1616.
- [22] C. Carstensen and S. Puttkammer, *Adaptive guaranteed lower eigenvalue bounds with optimal convergence rates*, preprint, arXiv:2203.01028, 2022.

- [23] H. Chen, X. Dai, X. Gong, L. He and A. Zhou, *Adaptive finite element approximations for Kohn-Sham models*, Multiscale Model. Simul., 12 (2014), 1828–1869.
- [24] H. Chen, X. Gong, L. He and A. Zhou, *Adaptive finite element approximations for a class of nonlinear eigenvalue problems in quantum physics*, Adv. Appl. Math. Mech., 3 (2011), 493–518.
- [25] H. Chen, L. He and A. Zhou, *Finite element approximations of nonlinear eigenvalue problems in quantum physics*, Comput. Methods Appl. Mech. Engrg., 200 (2011), 1846–1865.
- [26] L. Chen, *iFEM: an integrated finite element method package in MATLAB*, Technical Report, University of California at Irvine, 2009 (available at <https://github.com/lyc102/ifem>).
- [27] P. G. Ciarlet, *Finite element methods for elliptic problems*, North-Holland, Amsterdam, 1978.
- [28] X. Dai, L. He and A. Zhou, *Convergence and quasi-optimal complexity of adaptive finite element computations for multiple eigenvalues*, IMA J. Numer. Anal., 35 (2015), 1934–1977.
- [29] X. Dai, J. Xu and A. Zhou, *Convergence and optimal complexity of adaptive finite element eigenvalue computations*, Numer. Math., 110 (2008), 313–355.
- [30] L. Diening and C. Kreuzer, *Linear convergence of an adaptive finite element method for the p -Laplacian equation*, SIAM J. Numer. Anal., 46 (2008), 614–638.
- [31] D. Gallistl, *Adaptive nonconforming finite element approximation of eigenvalue clusters*. Comput. Methods Appl. Math., 14 (2014), 509–535.
- [32] D. Gallistl, *An optimal adaptive FEM for eigenvalue clusters*, Numer. Math., 130 (2015), 467–496.
- [33] D. Gallistl, *Morley finite element method for the eigenvalues of the biharmonic operator*, IMA J. Numer. Anal., 35 (2015), 1779–1811.
- [34] E. M. Garau and P. Morin, *Convergence and quasi-optimality of adaptive FEM for Steklov eigenvalue problems*, IMA J. Numer. Anal., 31 (2011), 914–946.
- [35] E. M. Garau, P. Morin and C. Zuppa, *Convergence of adaptive finite element methods for eigenvalue problems*, Math. Models Methods Appl. Sci., 19 (2009), 721–747.
- [36] J. P. García Azorero and I. Peral Alonso, *Existence and nonuniqueness for the p -Laplacian: nonlinear eigenvalues*, Comm. Partial Differential Equations, 12 (1987), 1389–1430.
- [37] S. Giani and I. G. Graham, *A convergent adaptive method for elliptic eigenvalue problems*, SIAM J. Numer. Anal., 47 (2009), 1067–1091.
- [38] R. Glowinski and J. Rappaz, *Approximation of a nonlinear elliptic problem arising in a non-Newtonian fluid model in glaciology*, ESAIM: Math. Model. Numer. Anal., 37 (2003), 175–186.
- [39] J. Horak, *Numerical investigation of the smallest eigenvalues of the p -Laplacian operator on planar domains*, Electr. J. Diff. Eqns, 132 (2011), 1–30.
- [40] J. Hu, Y. Huang and Q. Lin, *Lower bounds for eigenvalues of elliptic operators: By nonconforming finite element methods*, J. Sci. Comput., 61 (2014), 196–221.
- [41] J. Juutinen, P. Lindqvist and J. Manfredi, *The ∞ -eigenvalue problem*, Arch. Ration. Mech. Anal., 148 (1999), 89–105.

- [42] B. Kawohl and V. Fridman, *Isoperimetric estimates for the first eigenvalue of the p -Laplace operator and the Cheeger constant*, Comment. Math. Univ. Carol., 44 (2003), 659-667.
- [43] I. Kossaczky, *A recursive approach to local mesh refinement in two and three dimensions*, J. Comp. Appl. Math., 55 (1995), 275-288.
- [44] L. Lefton and D. Wei, *Numerical approximation of the first eigenpair of the p -Laplacian using finite elements and the penalty method*, Numer. Funct. Anal. Optim., 18 (1997), 389-399.
- [45] G. P. Leonardi, *An overview on the Cheeger problem*, New Trends in Shape Optimization (A. Pratelli and G. Leugering eds.), Birkhäuser, New York, 2015, 117-139.
- [46] A. Lê, *Eigenvalue problems for the p -Laplacian*, Nonlinear Anal., 64 (2006), 1057-1099.
- [47] P. Lindqvist, *On the equation $\operatorname{div}(|\nabla u|^{p-2}\nabla u) + \lambda|u|^{p-2}u = 0$* , Proceedings of the Amer. Math. Soc., 109 (1990), 157-164.
- [48] D. Liu and Z. Chen, *The adaptive finite element method for the p -Laplace problem*, Appl. Numer. Math., 152 (2020), 323-337.
- [49] W. Liu and N. Yan, *On quasi-norm interpolation error estimation and a posteriori error estimates for p -Laplacian*, SIAM J. Numer. Anal., 40 (2002), 1870-1895.
- [50] X. Liu, *A framework of verified eigenvalue bounds for self-adjoint differential operators*, Appl. Math. Comput., 267 (2015), 341-355.
- [51] F. Luo, Q. Lin and H. Xie, *Computing the lower and upper bounds of Laplace eigenvalue problem: by combining conforming and nonconforming finite element methods*, Sci. China Math., 55 (2012), 1069-1082.
- [52] R. H. Nochetto, K. G. Siebert and A. Veiser, *Theory of adaptive finite element methods: an introduction*, Multiscale, Nonlinear and Adaptive Approximation (R. A. DeVore and A. Kunothe eds.), Springer, New York, 2009, 409-542.
- [53] O. Savin, *C^1 -regularity for infinity harmonic functions in two dimensions*, Arch. Ration. Mech. Anal., 176 (2005), 351-361.
- [54] L. R. Scott and S. Zhang, *Finite element interpolation of nonsmooth functions satisfying boundary conditions*, Math. Comp., 54 (1990), 483-493.
- [55] R. Stevenson, *The completion of locally refined simplicial partitions created by bisection*, Math. Comp., 77 (2008), 227-241.
- [56] C. Traxler, *An algorithm for adaptive mesh refinement in n dimensions*, Computing, 59 (1997), 115-137.
- [57] A. Veiser, *Convergent adaptive finite elements for the nonlinear Laplacian*, Numer. Math., 92 (2002), 743-770.
- [58] R. Verfürth, *A Posteriori Error Estimation Techniques for Finite Element Methods*, Oxford University Press, Oxford, 2013.
- [59] Y. Yang, Z. Zhang and F. Lin, *Eigenvalue approximation from below using non-conforming finite elements*, Sci. China Math., 53 (2010), 137-150.

- [60] X. Yao and J. Zhou, *Numerical methods for computing nonlinear eigenpairs. I. Isohomogeneous cases*, SIAM J. Sci. Comput., 29 (2007), 1355-1374.